Investigating the propagation of helicon waves into magnetic mirrors using RF double probes and RF magnetic probes in high density plasma in MAGPIE

Juan F. Caneses[1] B. Blackwell[1]

[1]-Plasma Research Laboratory, The Australian National University (ANU)

18th November 2013, ORNL Oak Ridge, Tennessee

Australian National University

ansto

Outline

1. Motivation and introduction to the MAGPIE helicon device.
2. Diagnostics in MAGPIE
   A. Emphasis on the RF double probe technique
3. Measurements of helicon wave propagation into a magnetic mirror
   A. Axial field measurements
   B. Radial field measurements
4. Summary and Discussion
5. Additional work

The importance of Plasma-Surface Interaction:

Sources of Plasma Wall Interaction in a Fusion reactor:

- Radial particle and energy transport to the plasma facing components
- Plasma contact at the Divertor: energy and particle exhaust
- Neutron and fast particle fluxes to the wall
- Fast particle physics.
- Transient events such as ELMs

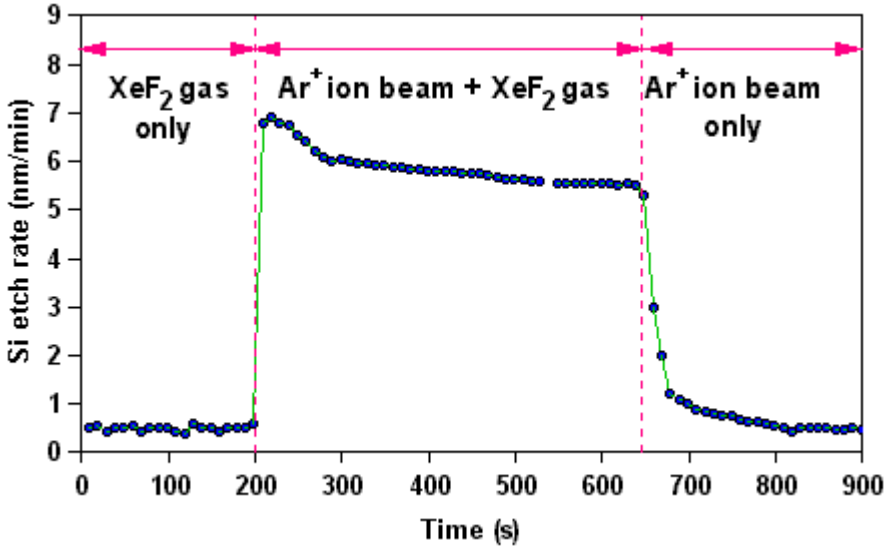

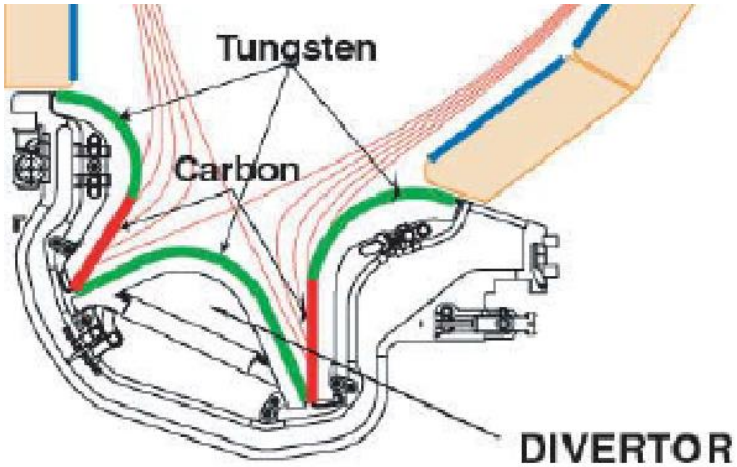

MAGPIE Device >>

MAGnetized Plasma Interaction Experiment (MAGPIE):

- Linear plasma device at the PRL to study fundamentals of Plasma-Material interactions relevant to Fusion devices.

Objectives:

- Basic Plasma-surface interaction physics.
- Approximates edge and Divertor plasmas.
- Material testing (ANSTO)
- Basic Plasma physics: Helicons

Most relevant:

1. Electrode-less RF plasma source
   - Helicon source
2. Non-uniform magnetic field
   - Enhances plasma density (Mori et al 2004)

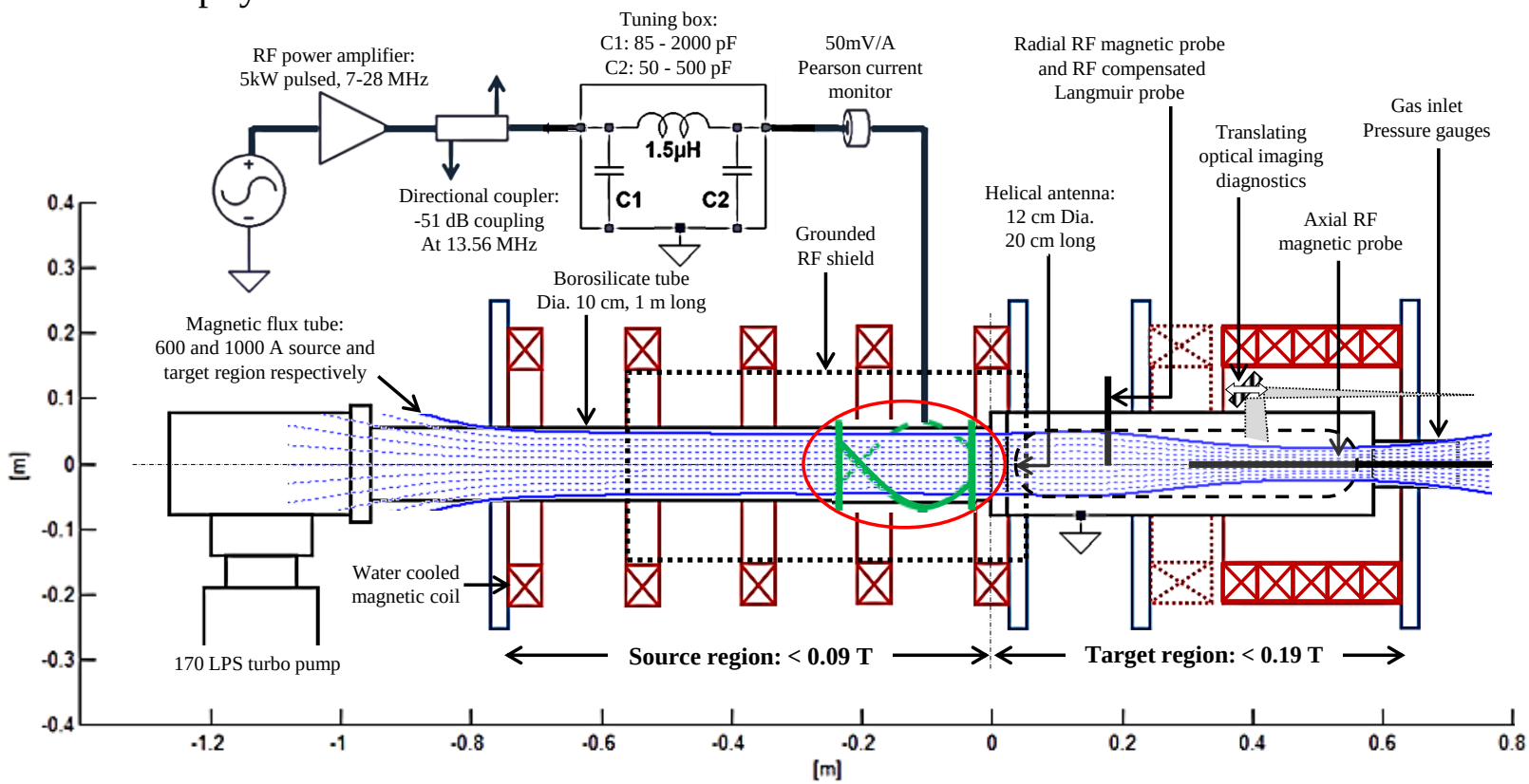

Parameter space >>

MAGnetized Plasma Interaction Experiment (MAGPIE):

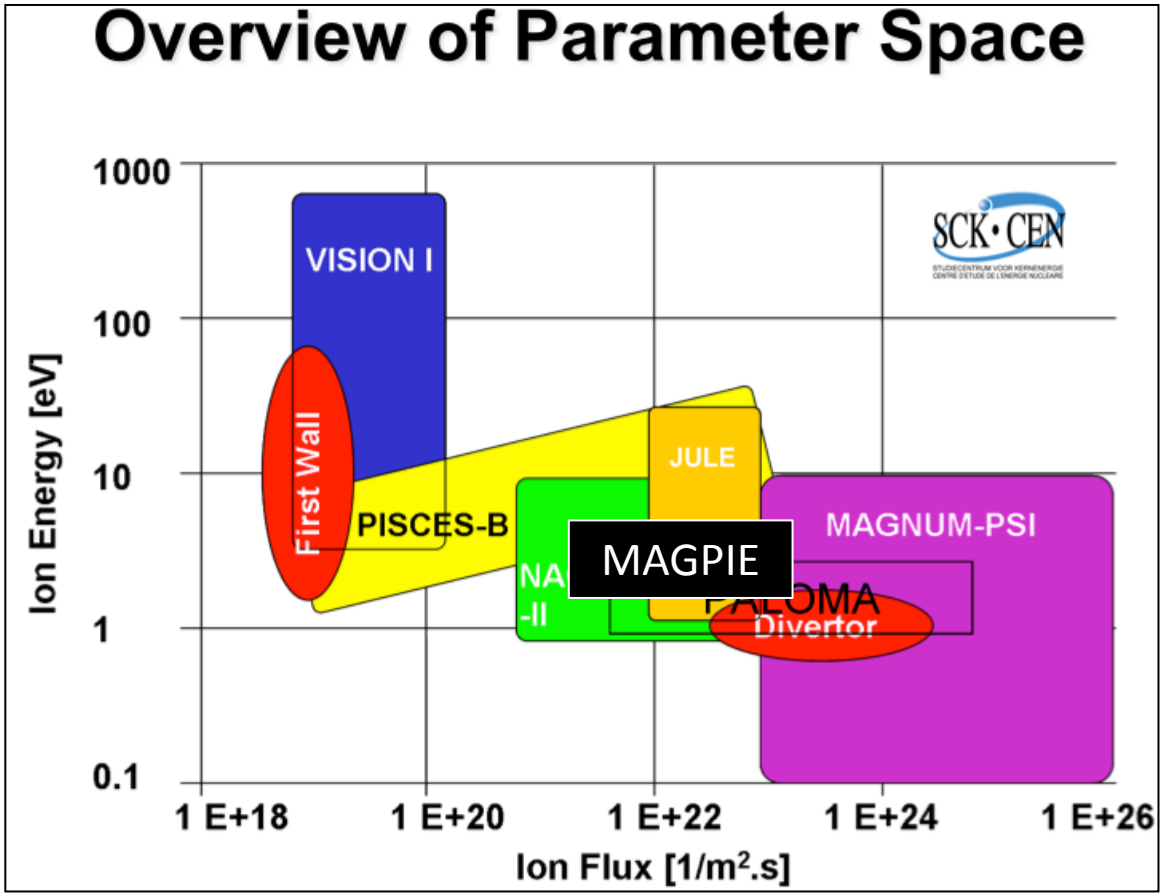

Target in MAGPIE:

Te ~ 5 eV, *ni* > 10^{19} m^{-3} *(in hydrogen)*

with thermal ion flux>2×10^{22} m^{-2}, and>10^{23} m^{-2} with bias.

Diagnostics >>

Diagnostics:

140 GHz Heterodyne polarization interferometer:

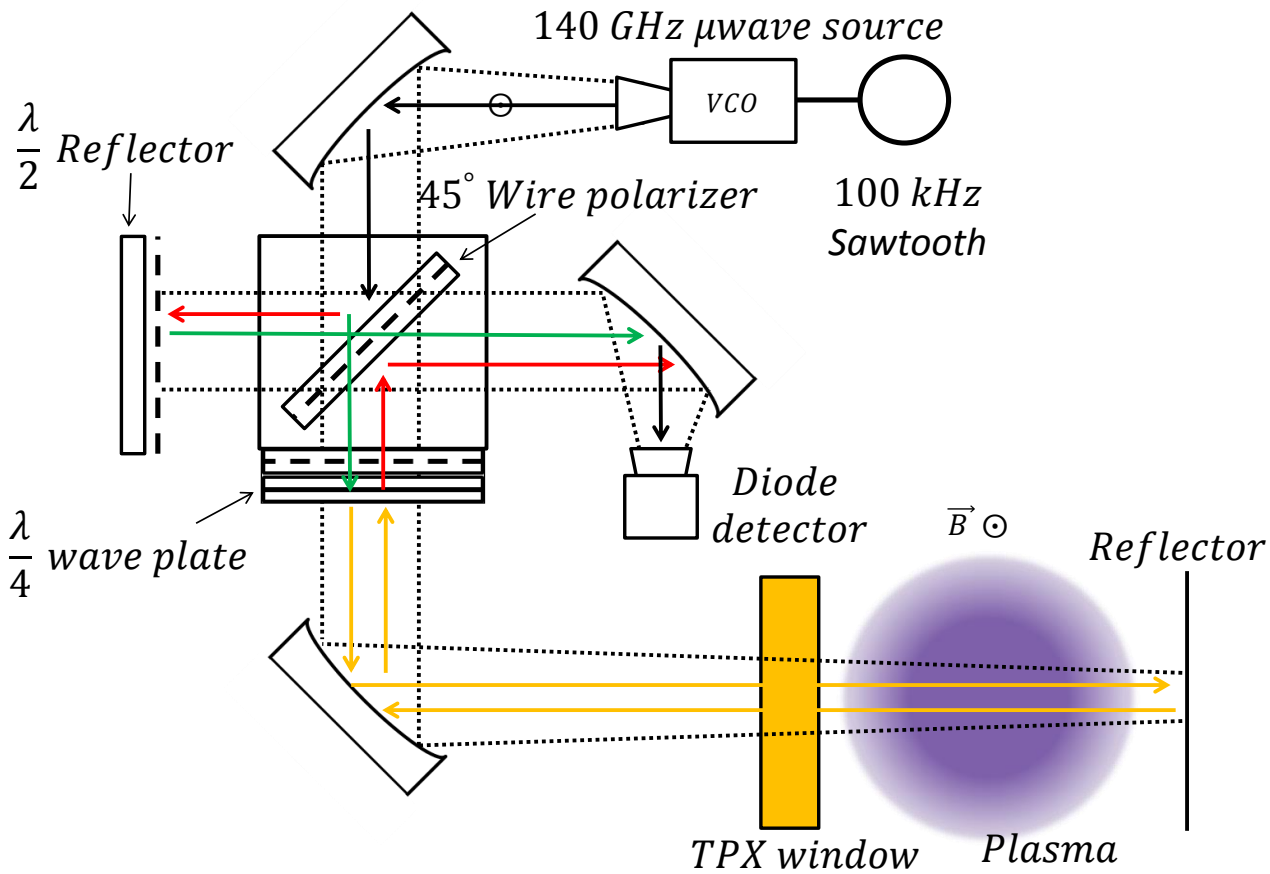

Symmetric RF double Langmuir probe:

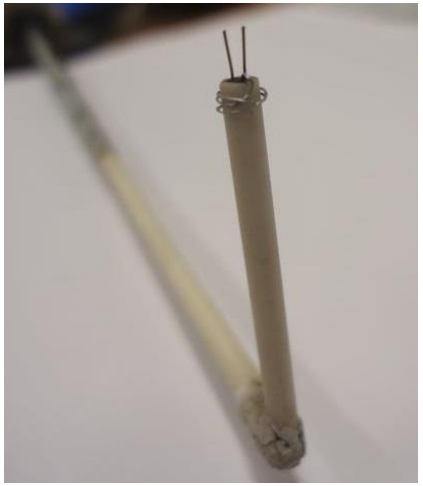

- 0.17 mm diam.
- 10 mm length
- 100 pF stray
- 30 kHz sweep
- 120 V_{pp}

Interferometer example >>

Interferometer: Density increase as a function of RF power

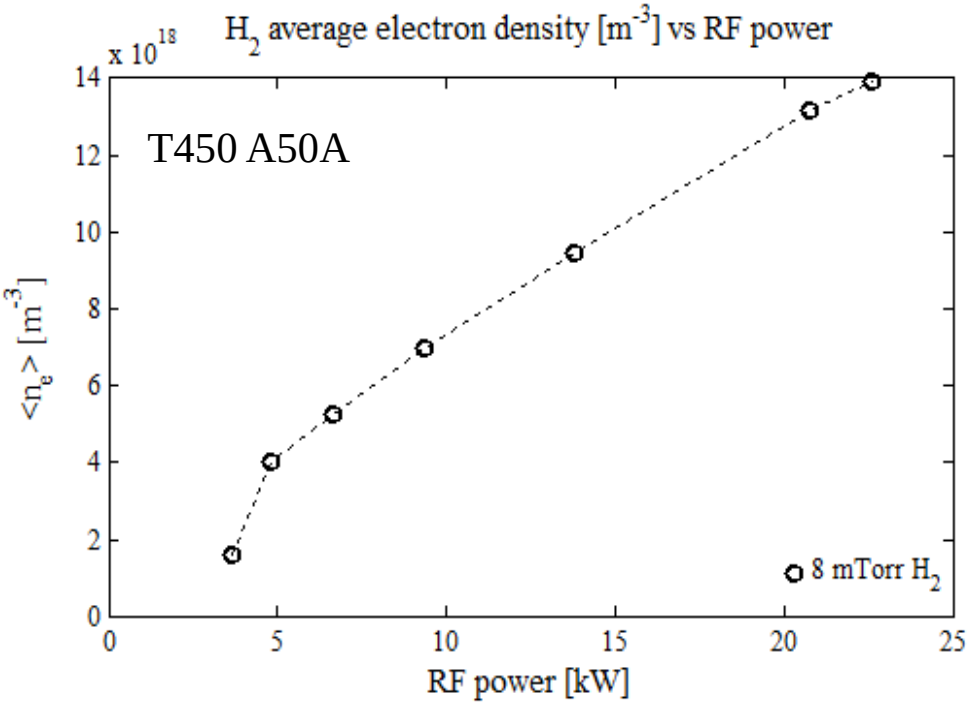

$$\langle n_e \rangle = \frac{1}{L}\int_0^L n_e(r)\,dr = -\left(\frac{2cn_c}{\omega L}\right)\Delta\phi$$

L is determined from experimentally measured ion density profiles.
In this case, L is approx. 20 cm

- Linear increase in density with RF power.
- High density transition above 4 kW.

- Pulsed operation to keep probes cool.
- Steady state achieved in approx. 0.5 mS at 8 mTorr
- Longer rise times for high pressures

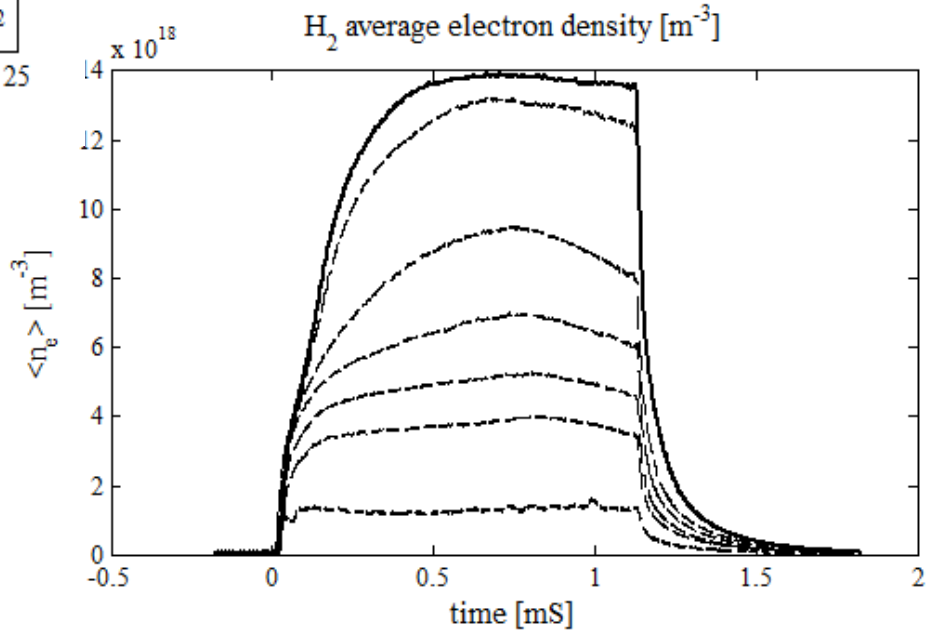

QI mixer and Bdot >>

Bdot probe: Quadrature detector RF magnetic probe

:

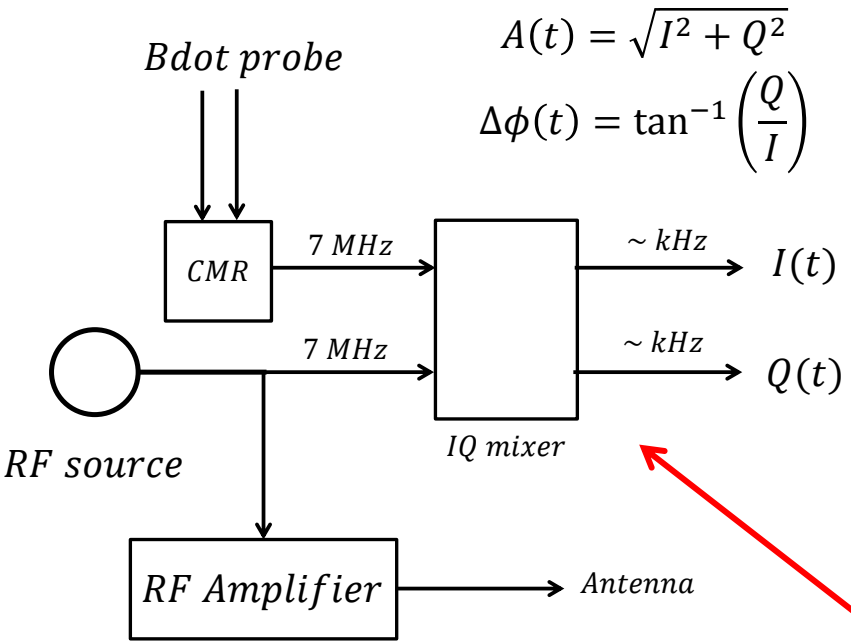

$$A(t) = \sqrt{I^2 + Q^2}$$

$$\Delta\phi(t) = \tan^{-1}\left(\frac{Q}{I}\right)$$

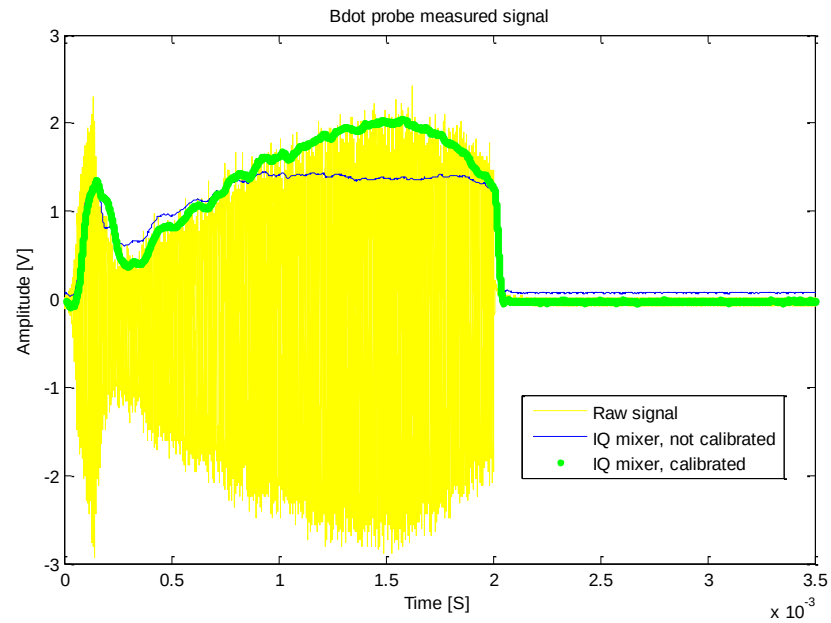

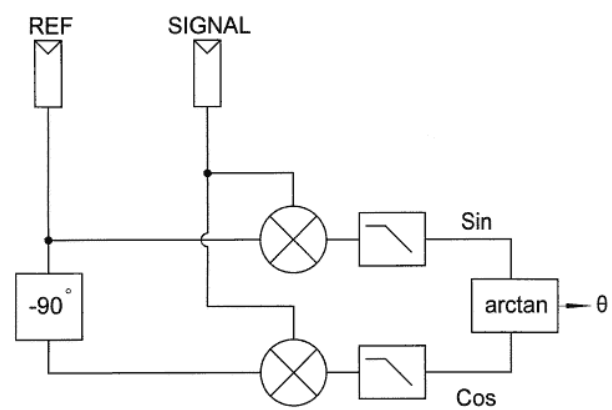

- As RF power and magnetic field is increased, helicon is very dynamic in time.
- Use IQ mixer to resolve over mS time scales

Double probe >>

Symmetric RF double Langmuir probe:

- Heat damage of RF compensated probes in MAGPIE
- Double probe has intrinsic RF compensation
  - How good?
- Double probe commonly implemented in literature

Important :

- Sheath expansion/potential dependant ion currents.
- Magnetization of current collection
- RF rectification effects

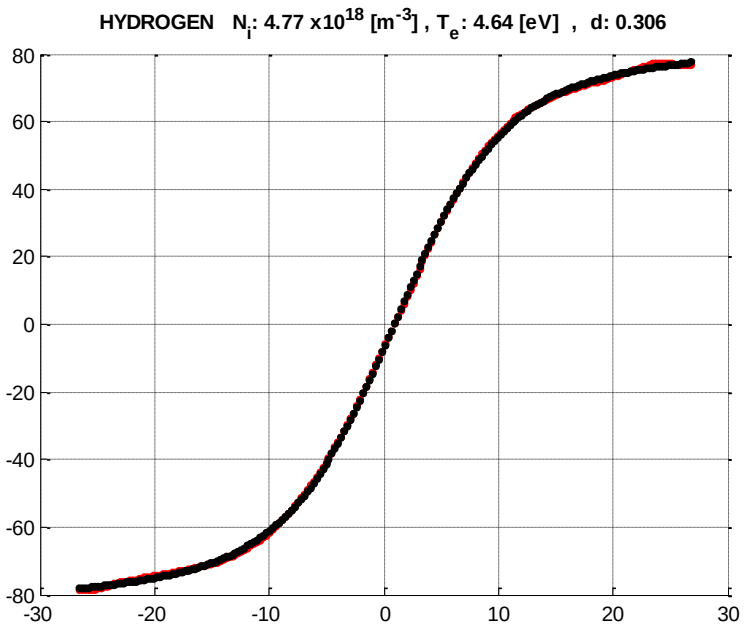

Model with sheath expansion

$$I(U) = I_+ \tanh\left(-\frac{(U-c)}{2T_e}\right) + M(U-c) + e$$

RF effects on double probe:

$$n_i = \frac{I_+}{0.61 e A_p C_s} + \Delta \boldsymbol{n_i} \qquad T_e = \frac{I_+}{2}\left(\frac{\partial I}{\partial V}\right)^{-1}_{V=0} + \Delta \boldsymbol{T_e}$$

$$\frac{\Delta \boldsymbol{n_i}}{\boldsymbol{n_i}} = \frac{m}{I_+}\left[\boldsymbol{\phi_B}\left(\frac{\omega\tau_+}{2}\right) + \Delta\phi_S - \ln\left(1 + \frac{m}{2I_+}|\Delta\phi|\right)\right]$$

$$\frac{\Delta \boldsymbol{T_e}}{\boldsymbol{T_e}} = \frac{m}{I_+}\left[(\boldsymbol{\phi_B}(\omega\tau_+) + 1)\right]$$

See Caneses YP8 92

Double probe model >>

RF compensation and floating probes:

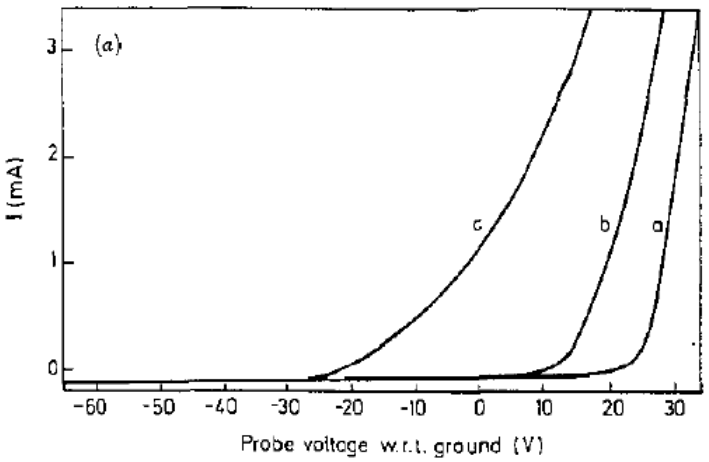

$$\phi_F = -\ln\left(\frac{I_e}{I_+}\right) - \phi_B \quad \phi_B = \ln\left[I_0\left(\frac{V_{RF}}{T_e}\right)\right]$$

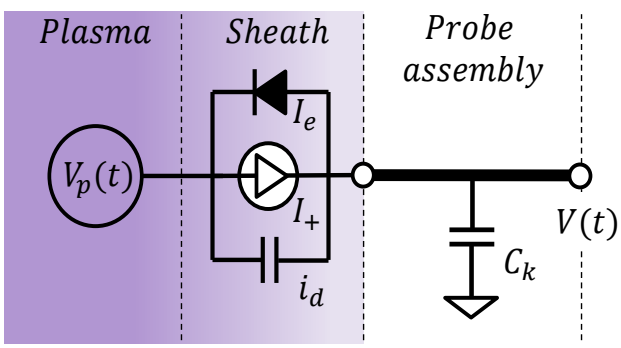

Passively driven floating probe model

Generalized floating probe model

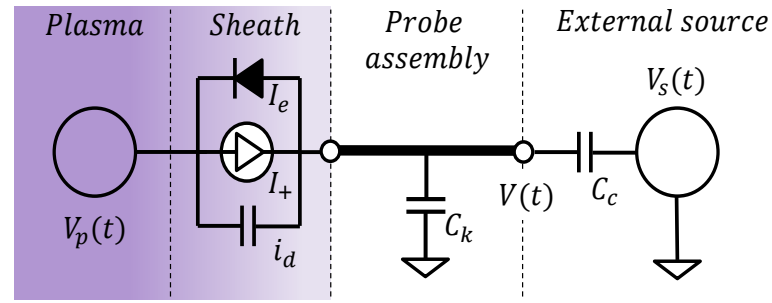

RF double probe model

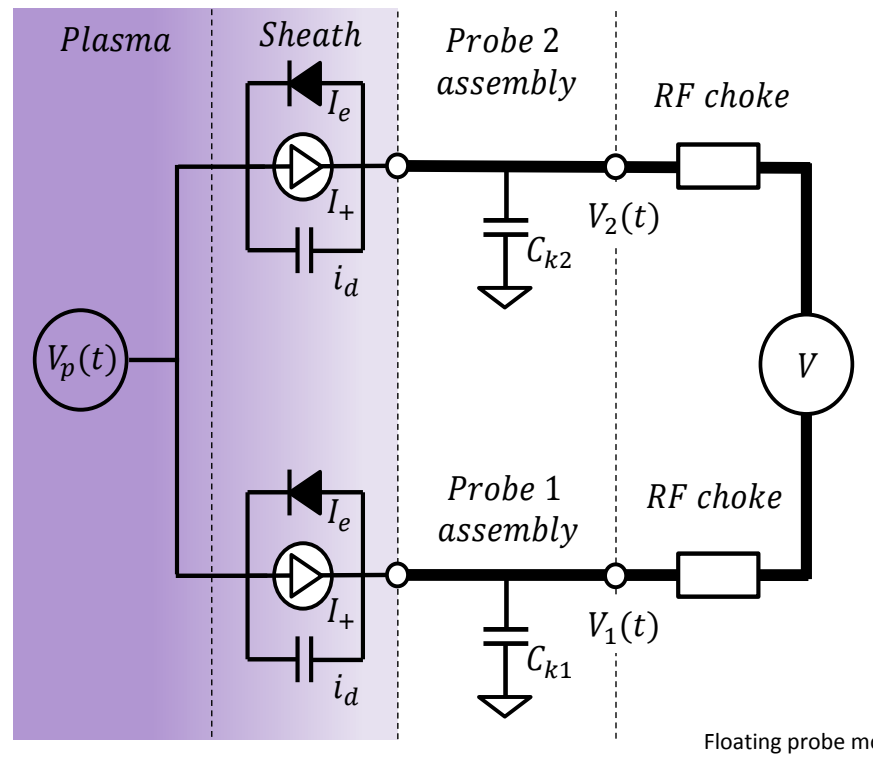

Floating probe model >>

Driven floating probe model:

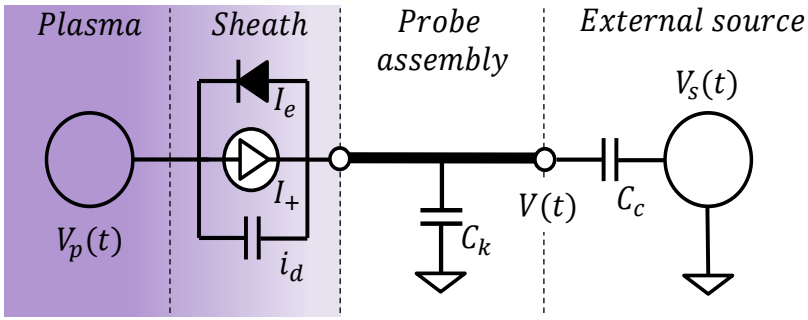

Generalized floating probe model

$$I = I_+ - I_e e^{\phi_0} e^{-\phi_p} + T_e C_s \frac{d}{dt}\phi_0 \qquad I = T_e C_k \frac{d}{dt}\phi_0 + T_e C_c \frac{d}{dt}(\phi_0 - \phi_s) \qquad \phi_0 = \left[\frac{V - V_p}{T_e}\right]$$

$$\boxed{\dot{\phi}_0(1-\alpha) + \frac{e^{\phi_0}}{\tau_e} e^{-\phi_p} - \frac{1}{\tau_+} = \beta\dot{\phi}_s - \alpha\dot{\phi}_p}$$

$$\frac{1}{\tau_+} = \frac{I_+}{T_e(C_k + C_c)} \qquad \frac{1}{\tau_e} = \frac{I_e}{T_e(C_k + C_c)} \qquad \phi_p = \frac{V_p}{T_e} \qquad \phi_s = \frac{V_s}{T_e} \qquad \beta = \left(\frac{C_c}{C_k + C_c}\right) \qquad \alpha = \left(\frac{C_s}{C_k + C_c}\right)$$

Solutions >>

Symmetric RF double Langmuir probe:

Full RF rectification

$$\phi_F = -\ln\left(\frac{I_e}{I_+}\right) - \phi_B \quad \phi_B = \ln\left[I_0\left(\frac{V_{RF}}{T_e}\right)\right]$$

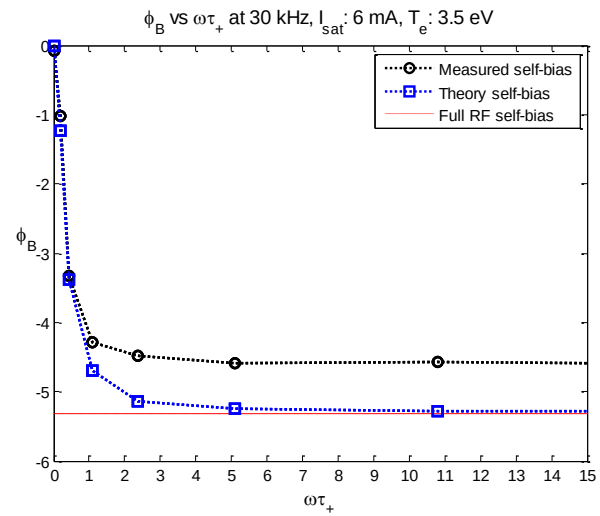

Passive driven solution:

$$\dot{\boldsymbol{\phi}}_{\mathbf{0}} + \frac{e^{\boldsymbol{\phi}_{\mathbf{0}}}}{\tau_e}\boldsymbol{e}^{-\boldsymbol{\phi}_{\boldsymbol{p}}} - \frac{\mathbf{1}}{\boldsymbol{\tau}_+} = 0 \quad \boldsymbol{\phi}_{\boldsymbol{p}} = \overline{\phi_p}\cos(\omega t)$$

$$\boxed{\phi_0 = -\ln\left(\frac{I_e}{I_+}\right) - \phi_B(\omega\boldsymbol{\tau}_+, \boldsymbol{\phi}_{\boldsymbol{p}})}$$

$$\boxed{\boldsymbol{\tau} = \frac{\boldsymbol{T_e C_k}}{\boldsymbol{I_+}}}$$

Actively driven solution:

$$\dot{\boldsymbol{\phi}}_{\mathbf{0}} + \frac{e^{\boldsymbol{\phi}_{\mathbf{0}}}}{\tau_e} - \frac{\mathbf{1}}{\boldsymbol{\tau}_+} = \boldsymbol{\beta}\dot{\boldsymbol{\phi}}_{\boldsymbol{s}} \quad \boldsymbol{\phi}_{\boldsymbol{s}} = \overline{\phi_s}\cos(\omega t)$$

$$\boxed{\phi_0 = \boldsymbol{\beta}\overline{\phi_s}\cos(\omega t) - \ln\left(\frac{I_e}{I_+}\right) - \phi_B(\omega\boldsymbol{\tau}_+, \boldsymbol{\phi}_{\boldsymbol{s}})}$$

$$\boxed{\phi_B(\omega\boldsymbol{\tau}_+, \boldsymbol{\phi}_{\boldsymbol{d}}) = \ln\left[I_0(\overline{\boldsymbol{\phi}_{\boldsymbol{d}}}) + 2\sum_{n=1}^{\infty} I_n(\overline{\boldsymbol{\phi}_{\boldsymbol{d}}})\left(\frac{\cos(n\omega t) + n\omega\boldsymbol{\tau}_+\sin(n\omega t)}{1 + (n\omega\boldsymbol{\tau}_+)^2}\right)\right] \quad \omega\tau_+ = \frac{R_{sh}}{Z_{stray}}}$$

Verification >>

Symmetric RF double Langmuir probe:

Experimental setup:

A- Rationale:

- Symmetry between the passively and actively driven probes solutions .
- Main motivation is to provide a model by which we can assess the RF compensation of a double probe.
- Indirectly test solution of passively driven model with actively driven setup.
- Experimental setup (H_2 $6x10^{17}$ m^{-3} and 3.5 eV) leads to ion plasma frequency of ~ 160 MHz. Thus operation below 15 MHz considered as DC sheath dynamics.

B- Apparatus:

- MAGPIE helicon plasma source [6]
- H_2 2.5 kW at 6 mTorr and 20 mT
- Capacitively coupled active drive: 30 kHz 50 V_{pp}, 0.5 to 100nF
- Probe stray capacitance 100 pF, maximum sheath capacitance ~ 2 pF based on Child-Langmuir sheath equations

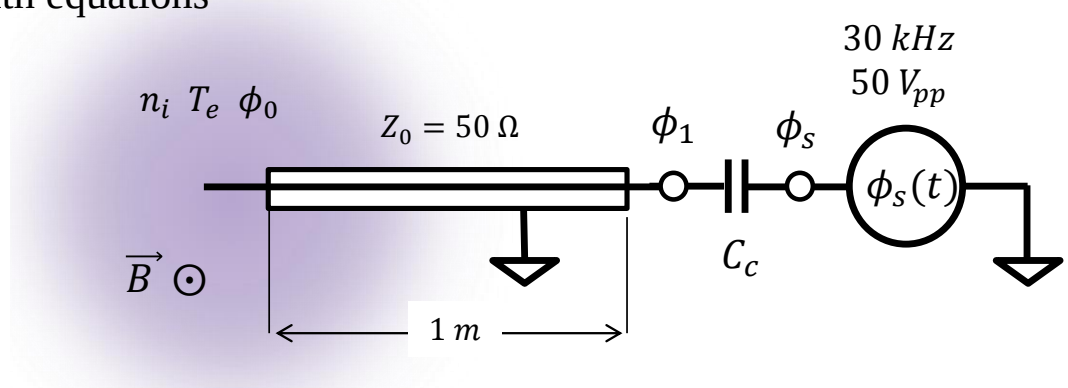

Results >>

Symmetric RF double Langmuir probe:

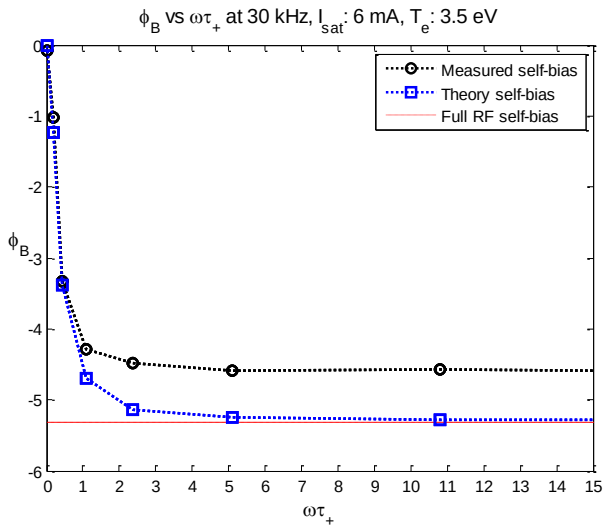

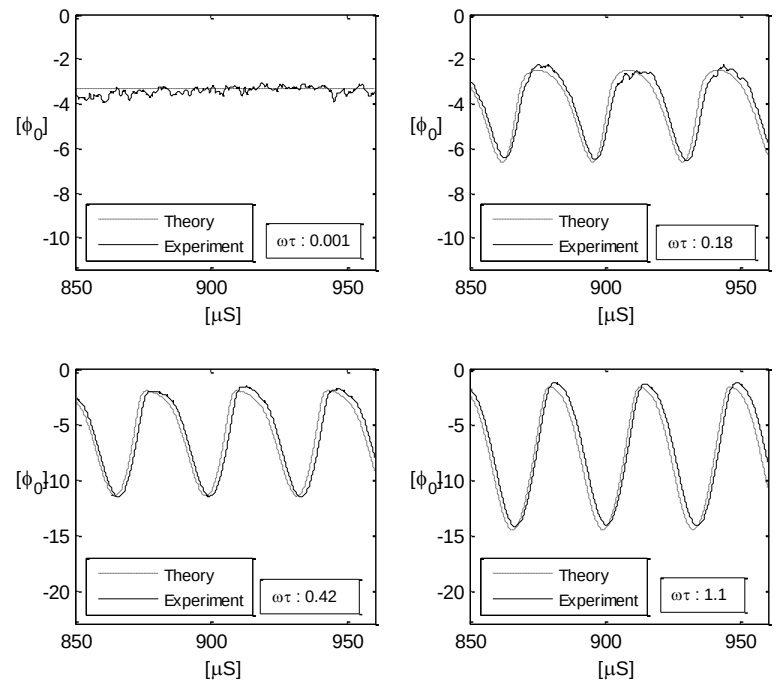

Results:

I- Probe potential waveforms and self-bias:

Discussion:

I- Self-bias in floating probes:

Experiments indicate that self-bias for floating probes can be described with the expressions presented.

For values of $\omega\tau_+$ much less the one, the probe is at the floating potential. And ϕ_B takes the form of the driving source, and the sheath exhibits DC sheath dynamics. For values equal or greater than one full sheath rectification occurs and the probe attains the full self bias potential.

In regards to the passive driven probe and RF compensation of floating probes, values of $\omega\tau_+ \ll 1$ allow probe surface to follow the plasma potential oscillations so that the sheath potential difference is stationary.

Implications on double probes>>

Symmetric RF double Langmuir probe:

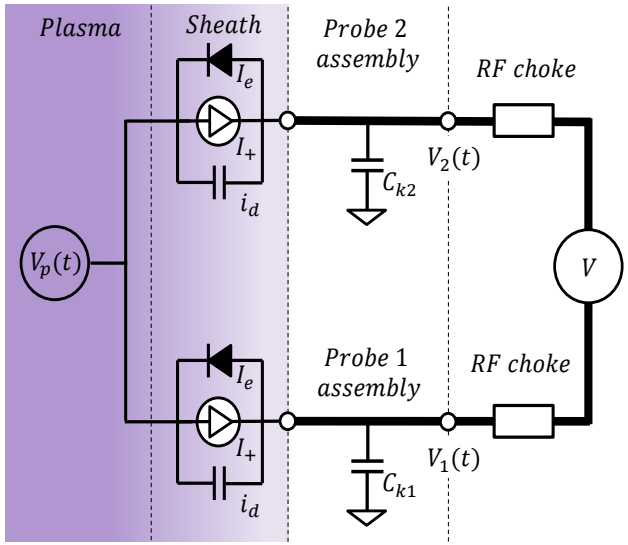

RF double probe model

$$I_{1,DC}(\Delta\phi) = I_{+1}\tanh\left(\frac{\Delta\phi}{2}\right) + \left(\frac{I_{+1} - I_{+2}}{e^{\Delta\phi} + 1}\right)$$

$$\dot{\boldsymbol{\phi}}_{\mathbf{n}} + \frac{e^{\boldsymbol{\phi}_{\mathbf{n}}}}{\tau_e}\boldsymbol{e}^{-\boldsymbol{\phi}_p} - \frac{\mathbf{1}}{\boldsymbol{\tau}_+} = 0 \qquad \boldsymbol{\phi}_{\boldsymbol{p}} = \overline{\phi_p}\cos(\omega t)$$

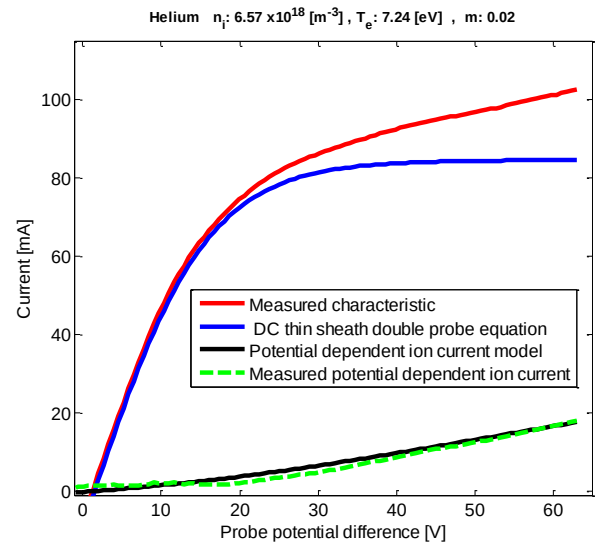

$$n_i = \frac{I_+}{0.61eA_pC_s} + \Delta\boldsymbol{n_i} \qquad T_e = \frac{I_+}{2}\left(\frac{\partial I}{\partial V}\right)^{-1}_{V=0} + \Delta\boldsymbol{T_e}$$

$$\frac{\Delta\boldsymbol{T_e}}{\boldsymbol{T_e}} = \frac{m}{I_+}[(\boldsymbol{\phi_B}(\omega\tau_+) + 1)]$$

$$\frac{\Delta\boldsymbol{n_i}}{\boldsymbol{n_i}} = \frac{m}{I_+}\left[\boldsymbol{\phi_B}\left(\frac{\omega\tau_+}{2}\right) + \Delta\phi_S - \ln\left(1 + \frac{m}{2I_+}|\Delta\phi|\right)\right]$$

$$\phi_B(\omega\boldsymbol{\tau}_+, \boldsymbol{\phi_d}) = \ln\left[I_0(\overline{\boldsymbol{\phi_d}}) + 2\sum_{n=1}^{\infty} I_n(\overline{\boldsymbol{\phi_d}})\left(\frac{\cos(n\omega t) + n\omega\boldsymbol{\tau}_+\sin(n\omega t)}{1 + (n\omega\boldsymbol{\tau}_+)^2}\right)\right] \qquad \omega\tau_+ = \frac{R_{sh}}{Z_{stray}} = \frac{\boldsymbol{\omega T_e C_k}}{\boldsymbol{I_+}}$$

Benchmarking >>

Validating double Langmuir probe:

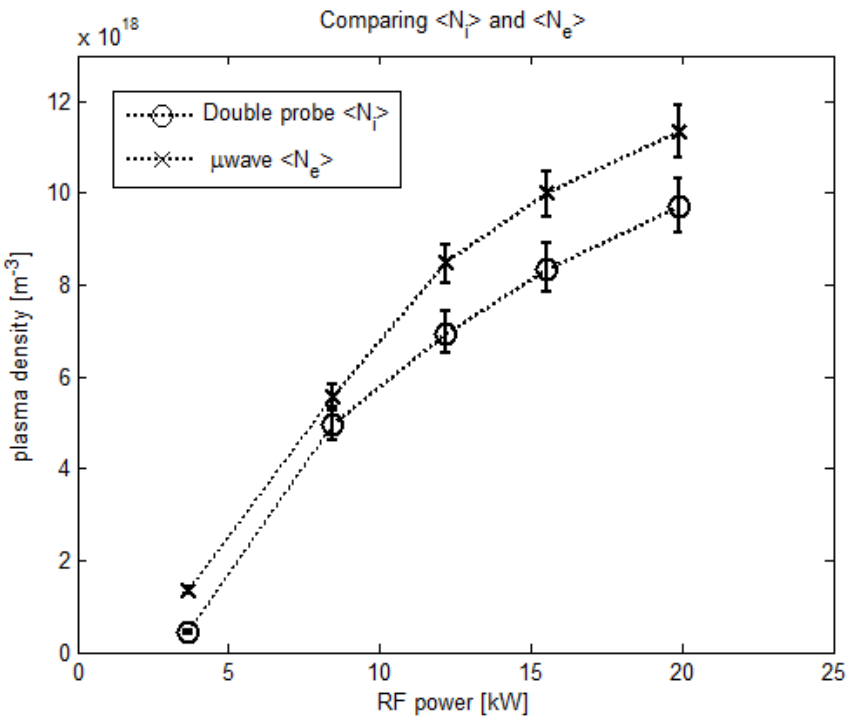

Ion and electron saturation currents parallel and perpendicular to magnetic field at standard magnetic field
Diam.: 0.17 mm, 10 mm length
50 to 180 mTesla

- H_2 plasma density (8 mTorr) and magnetization as shown in right figure.
- Double probe and interferometer measurement at same location.

Ratio of perpendicular to axial saturation current

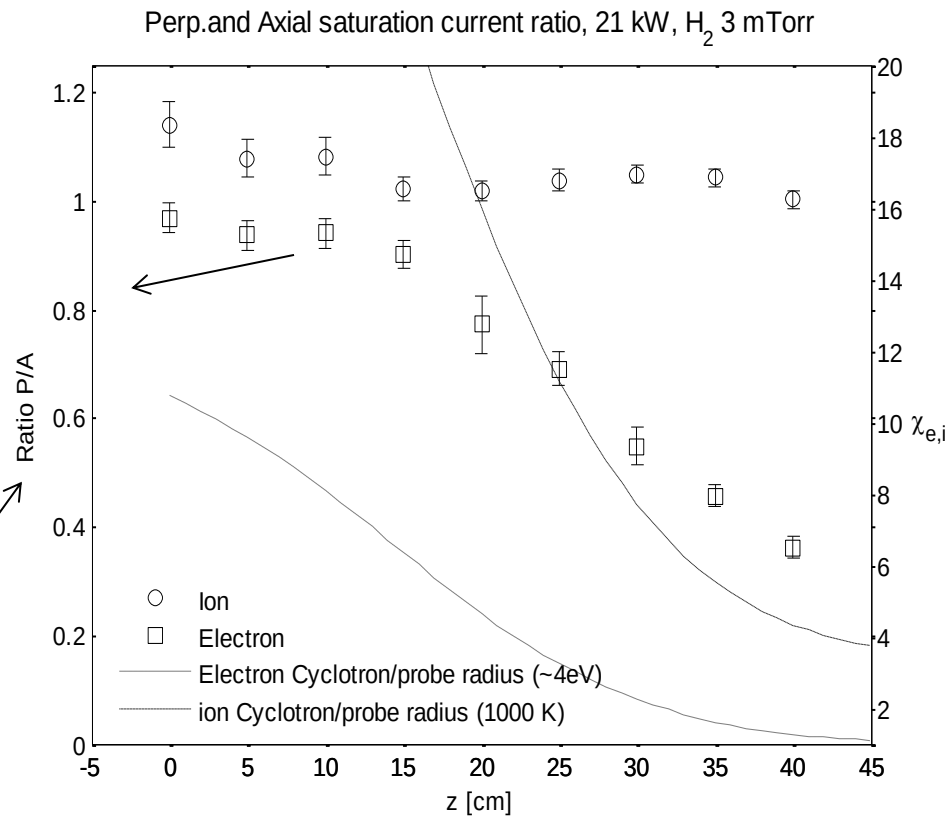

Axial position in MAGPIE

Experimental setup>>

Experimental setup:

Diagnostics: RF Double Langmuir probe and RF magnetic probes

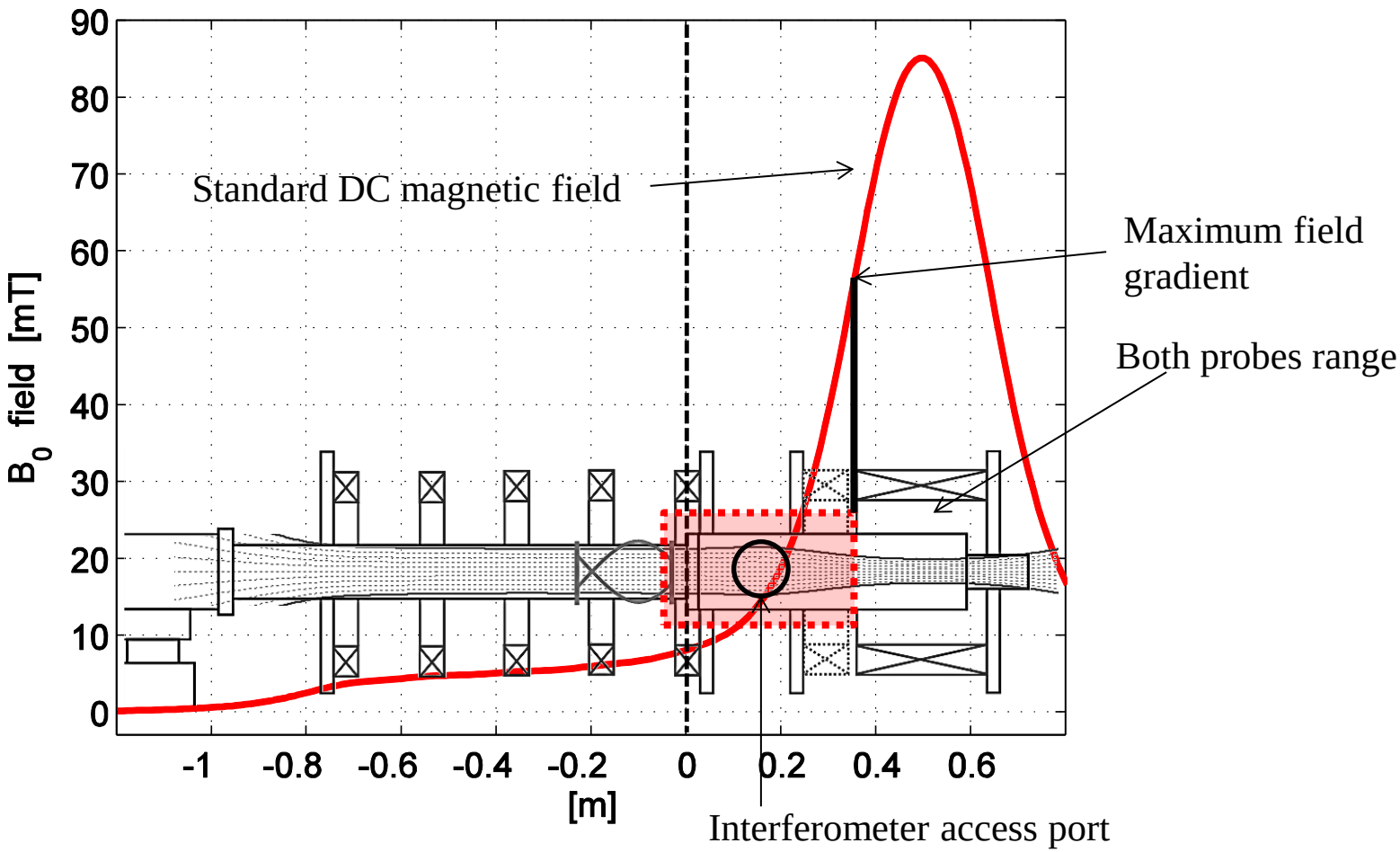

Helicon wave and plasma fields

Magnetic geometry:

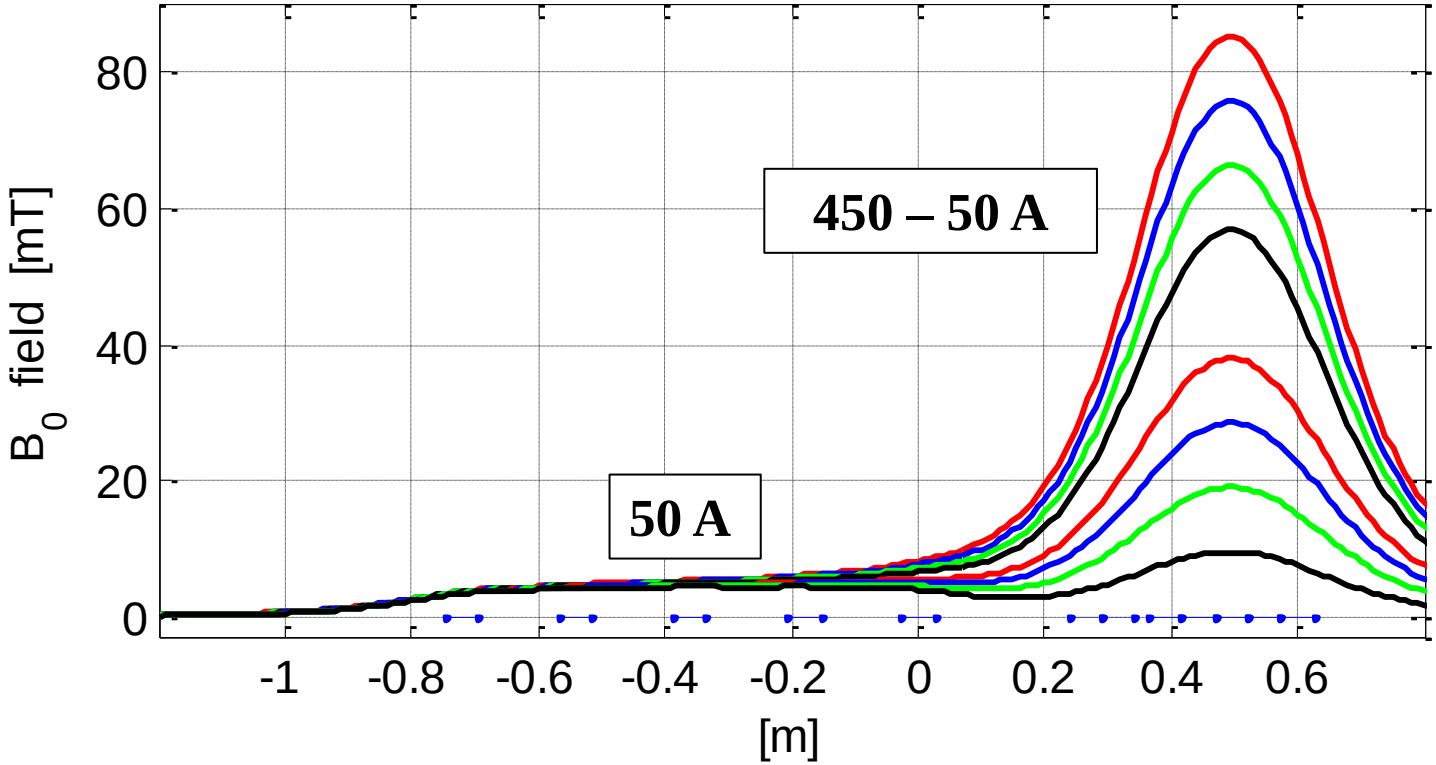

Axial measurements >>

Axial field measurements

Increasing the magnetic mirror for constant RF power leads to:

- Increase in ion density
- Decrease in electron temperature
- Excitation of high order radial modes

T450A S50A at 21 kW

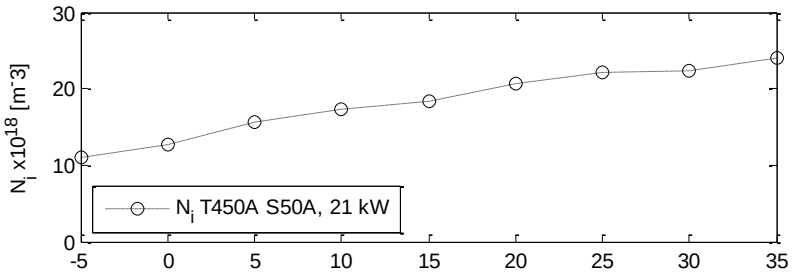

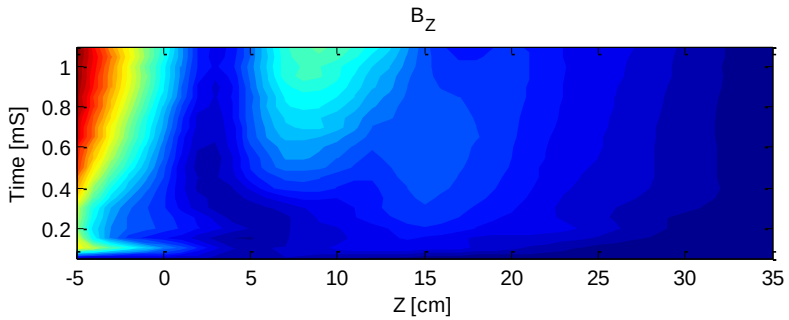

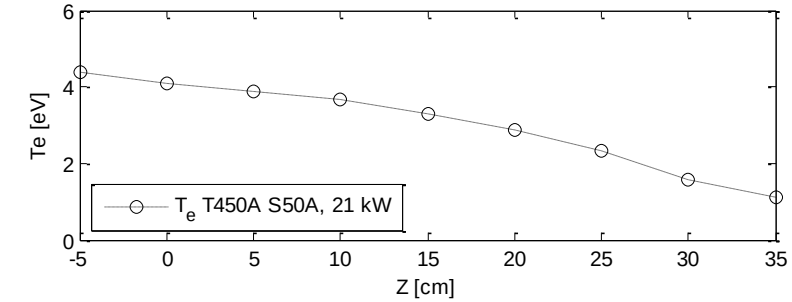

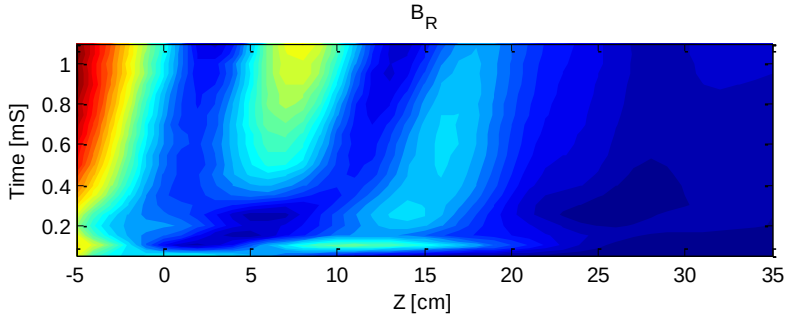

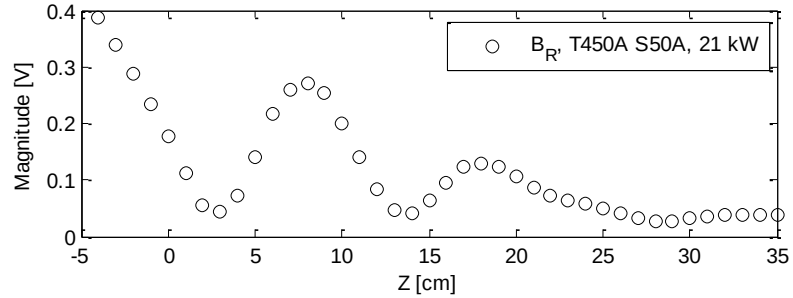

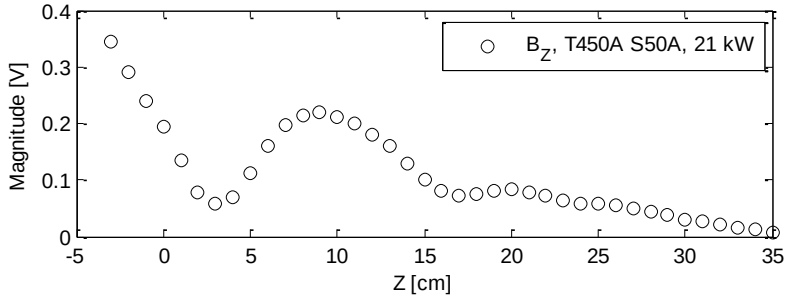

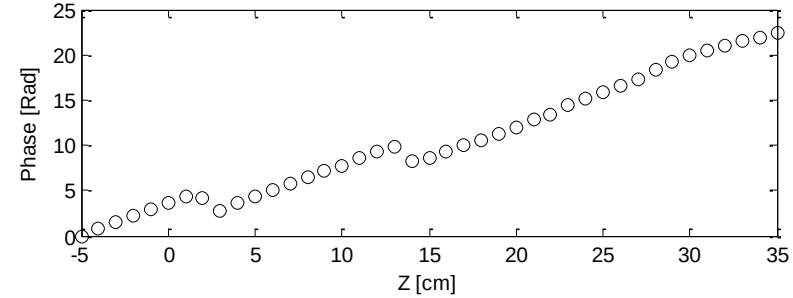

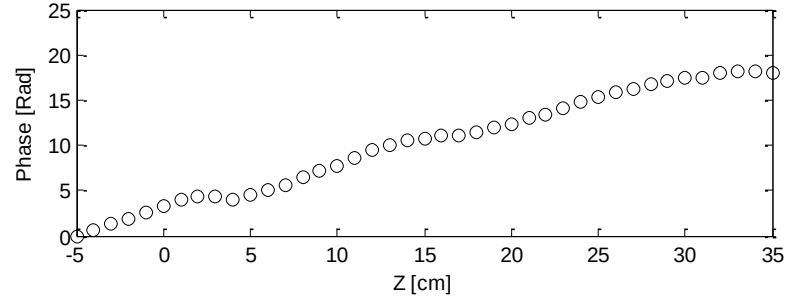

T400A S50A at 21 kW

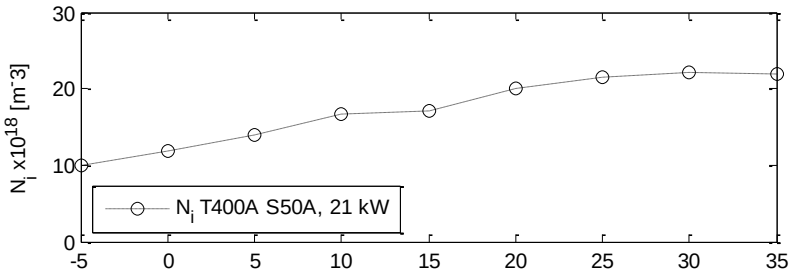

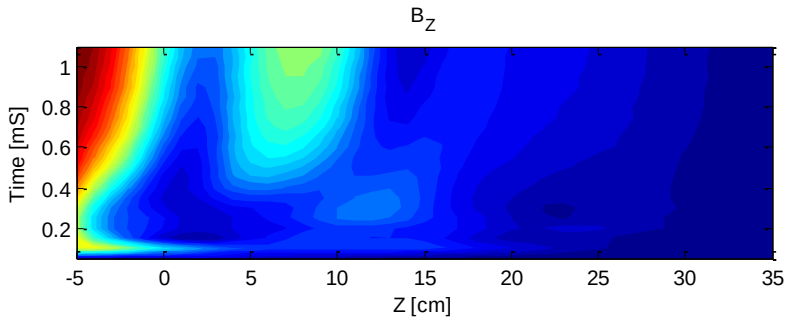

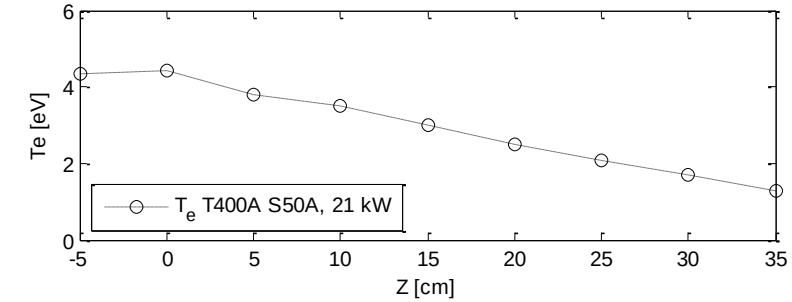

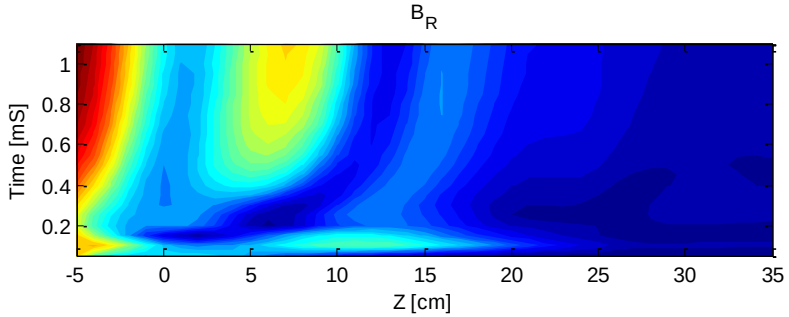

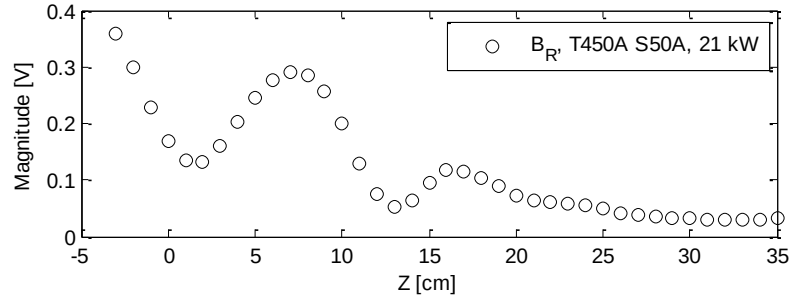

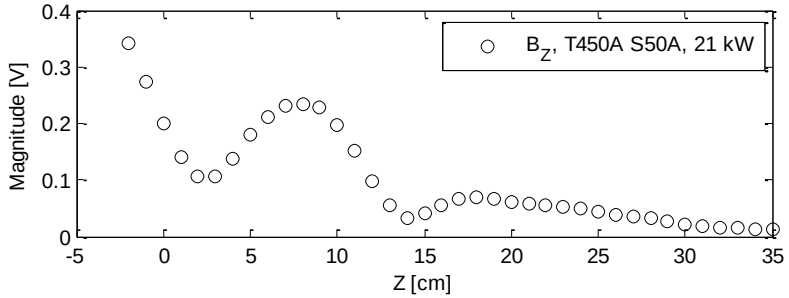

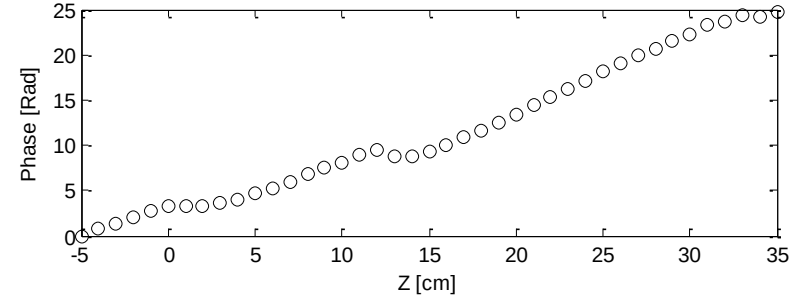

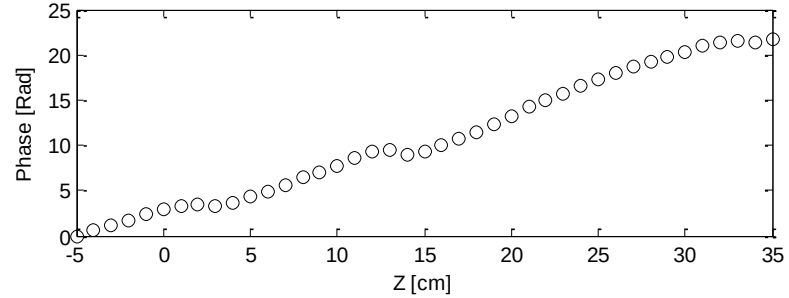

T350A S50A at 21 kW

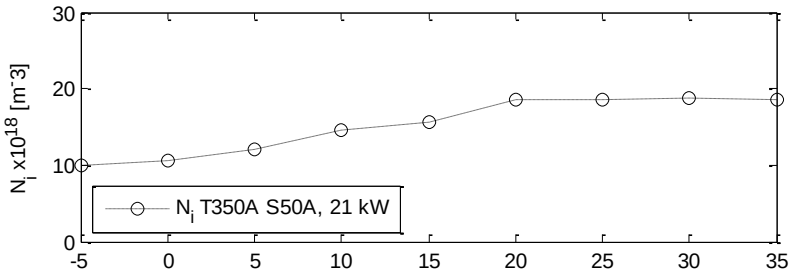

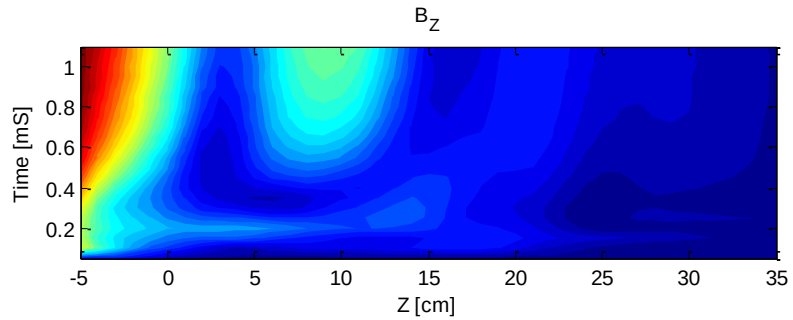

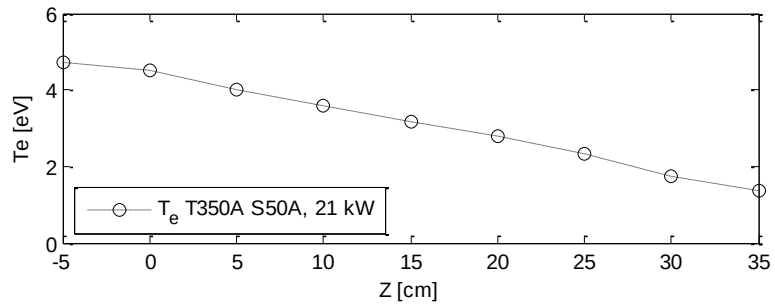

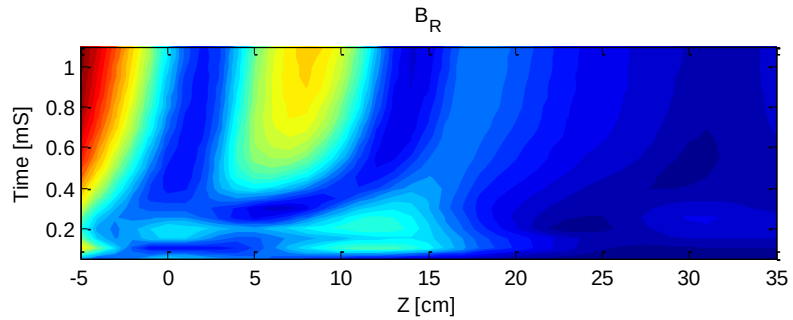

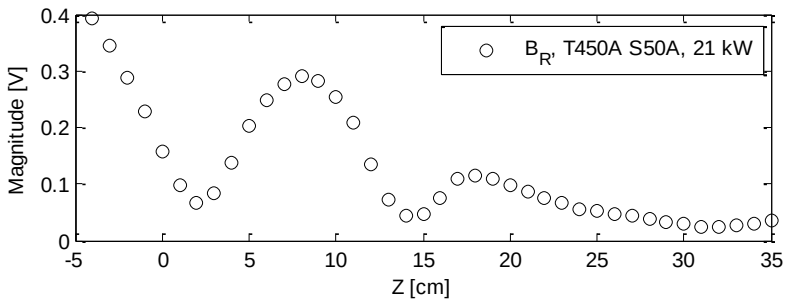

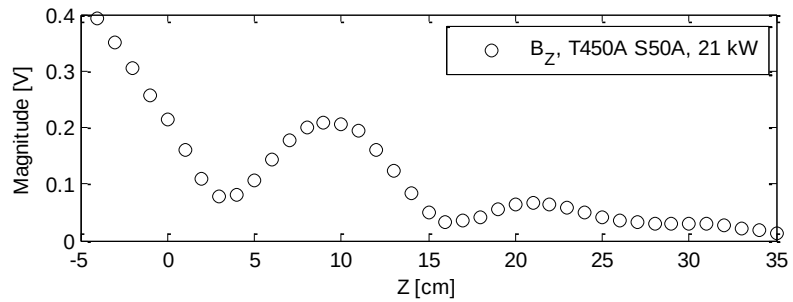

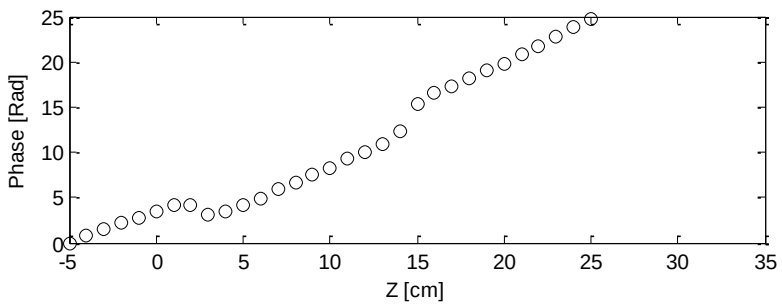

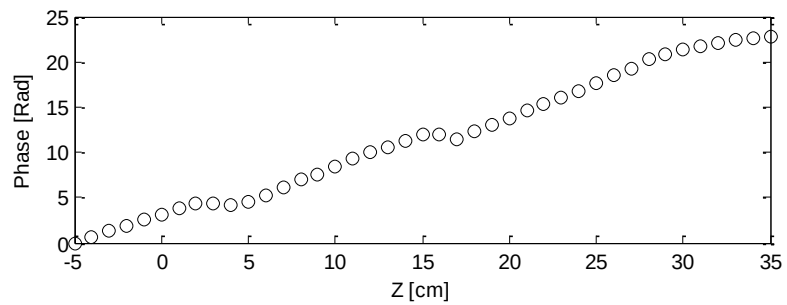

T300A S50A at 21 kW

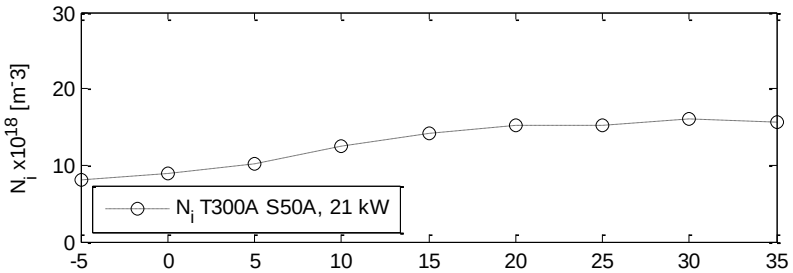

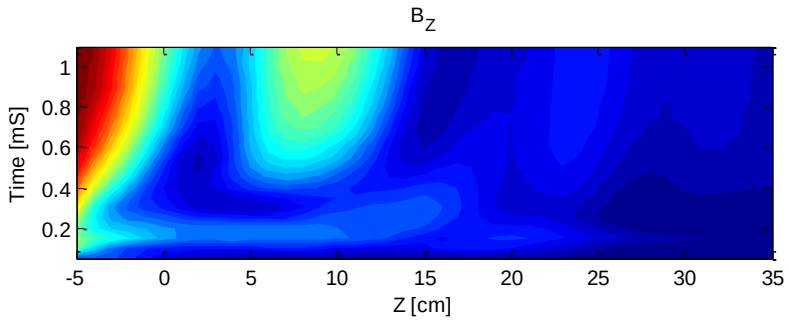

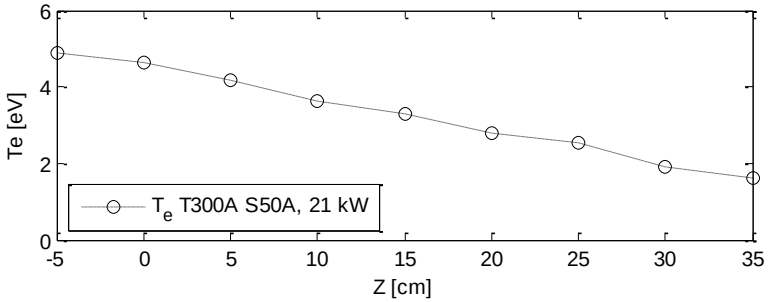

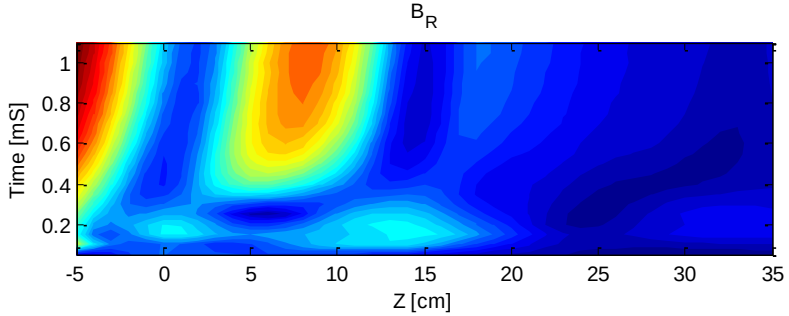

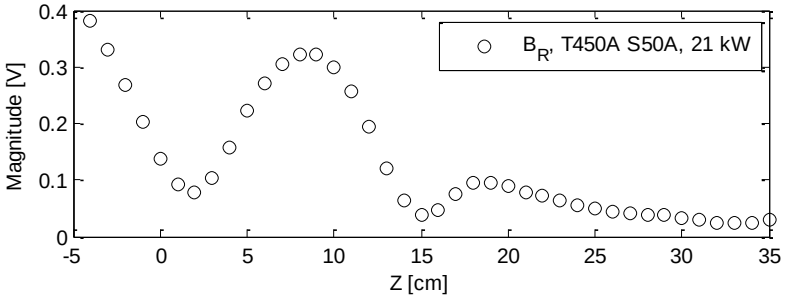

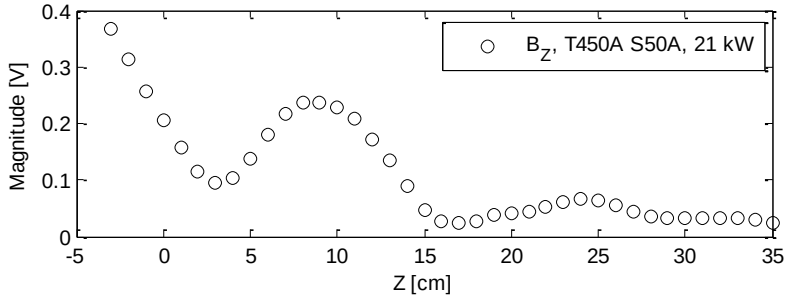

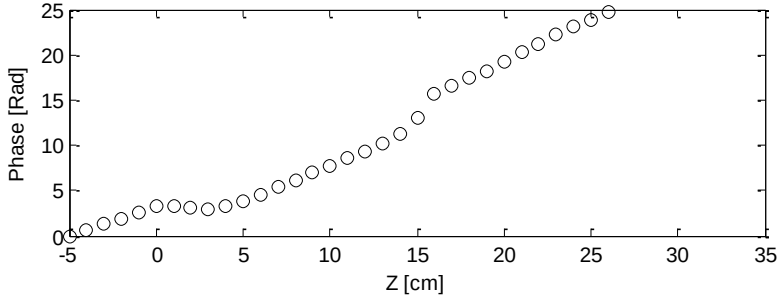

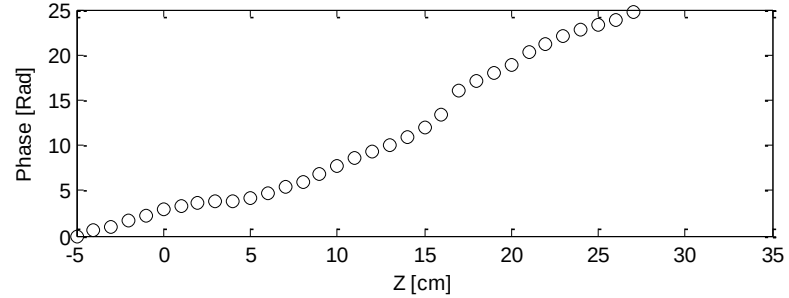

T200A S50A at 21 kW

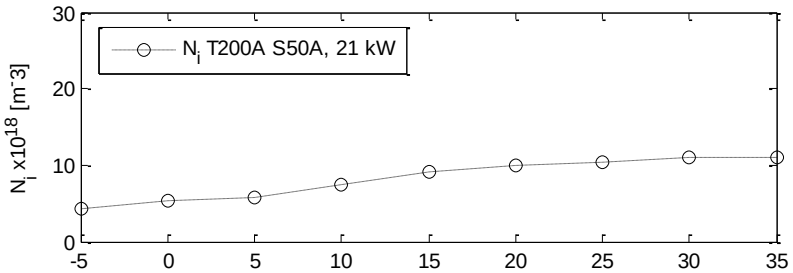

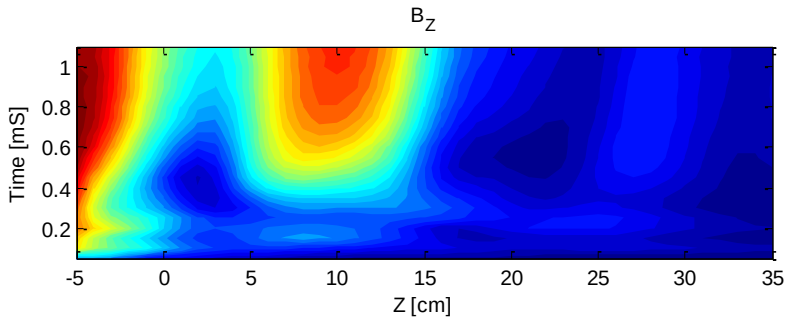

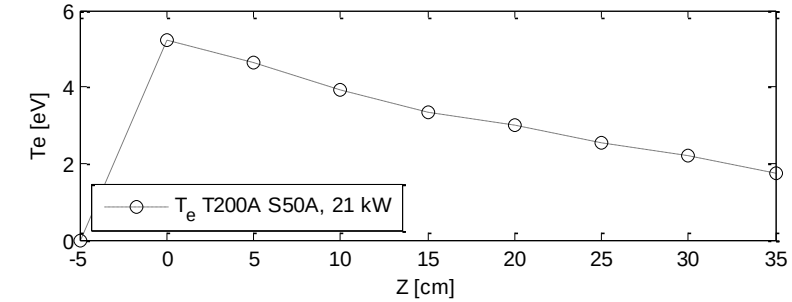

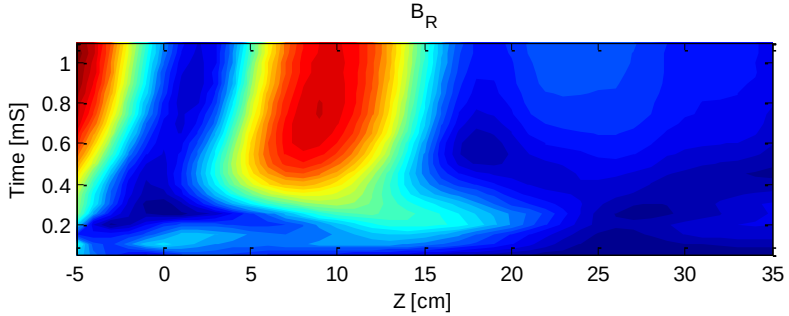

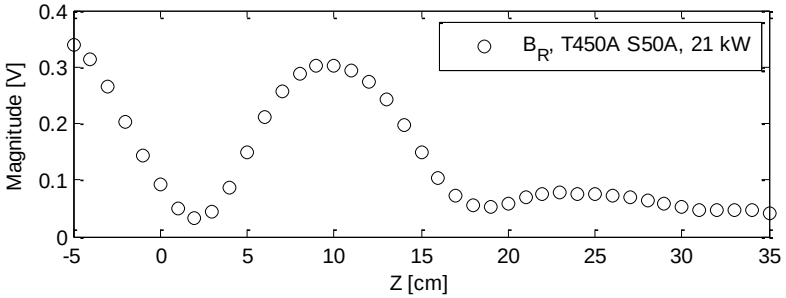

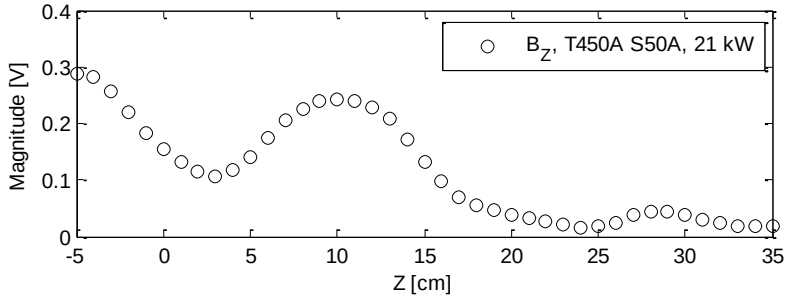

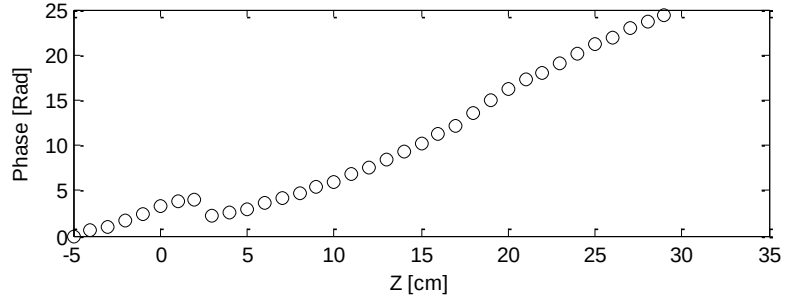

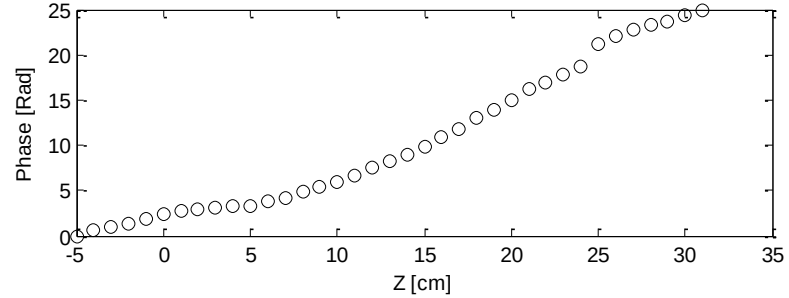

T150A S50A at 21 kW

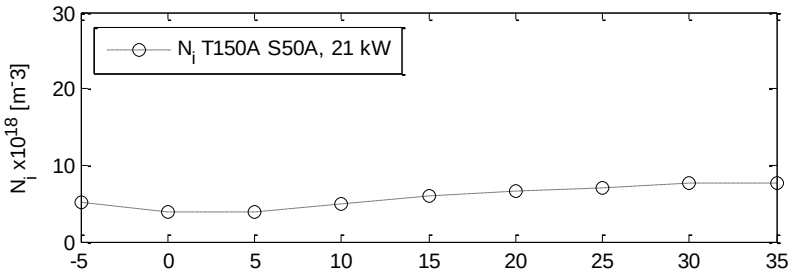

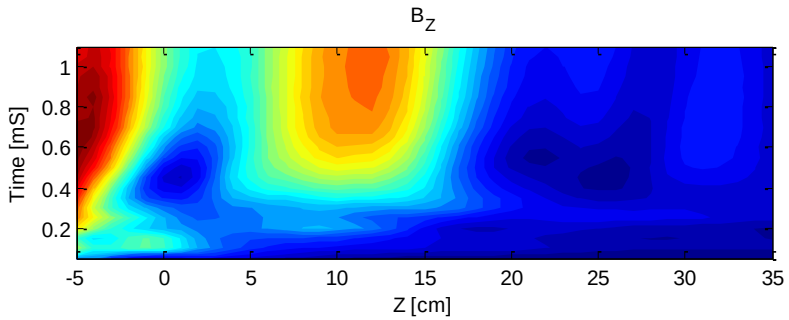

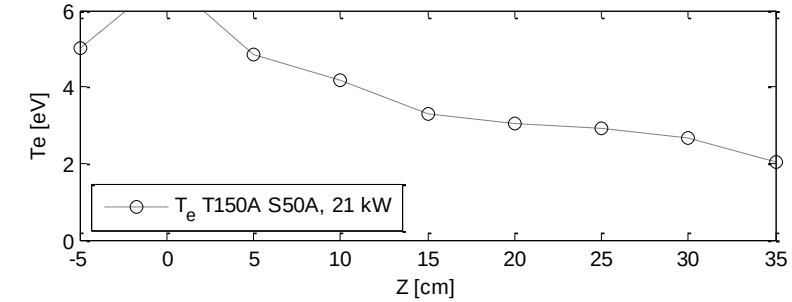

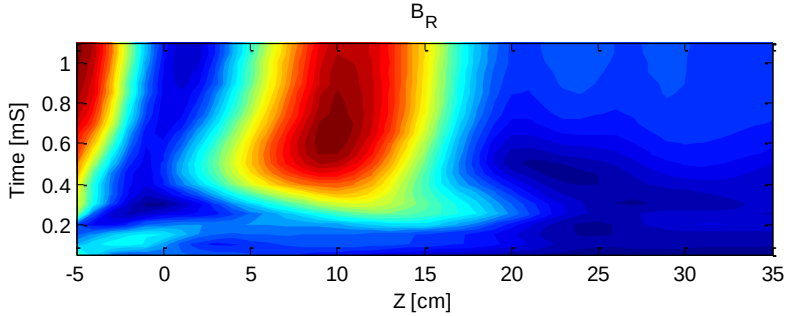

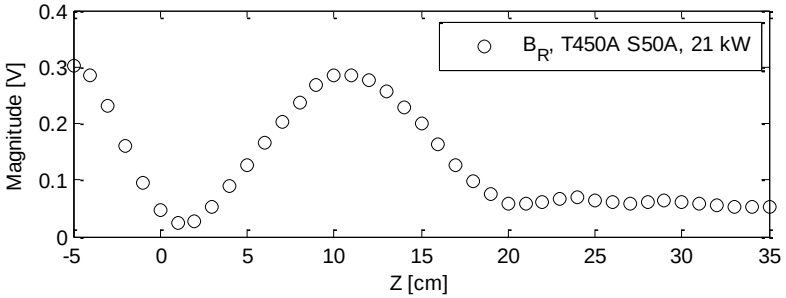

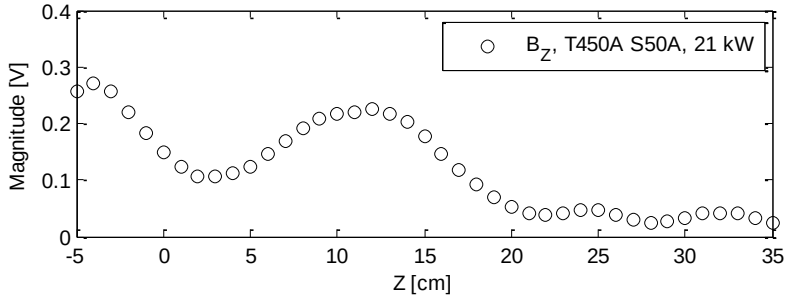

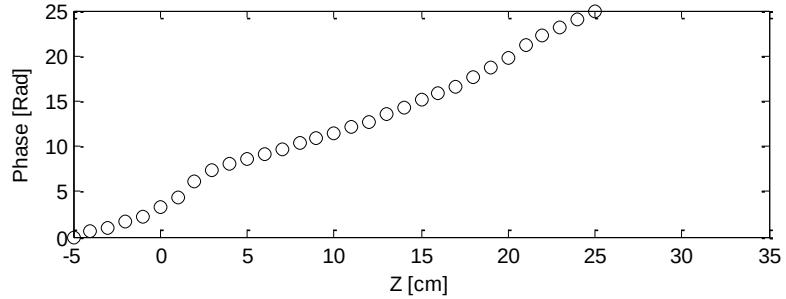

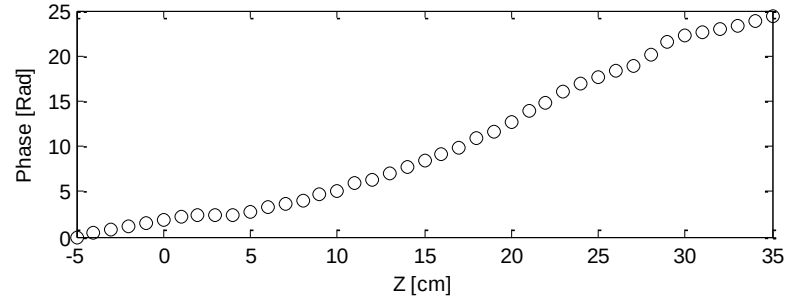

T100A S50A at 21 kW

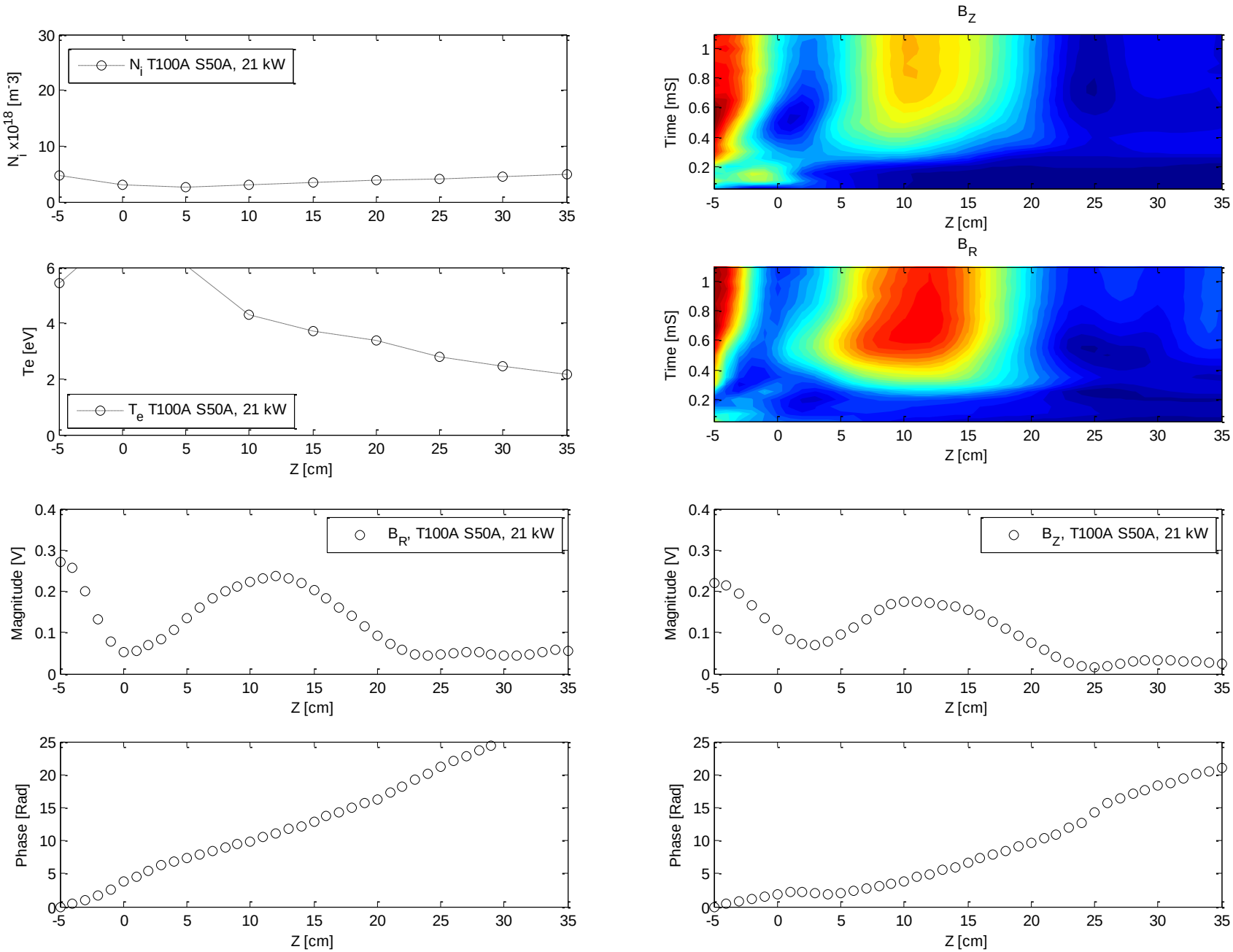

T050A S50A at 21 kW

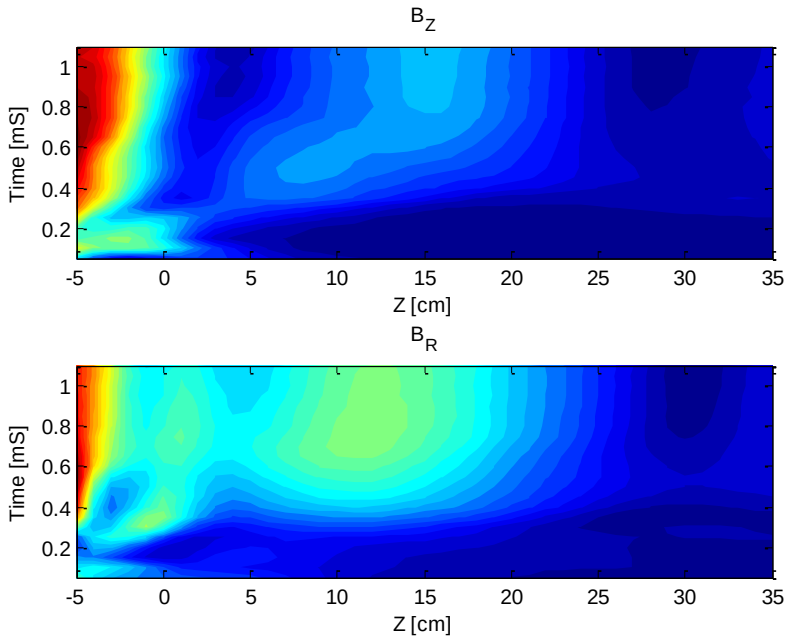

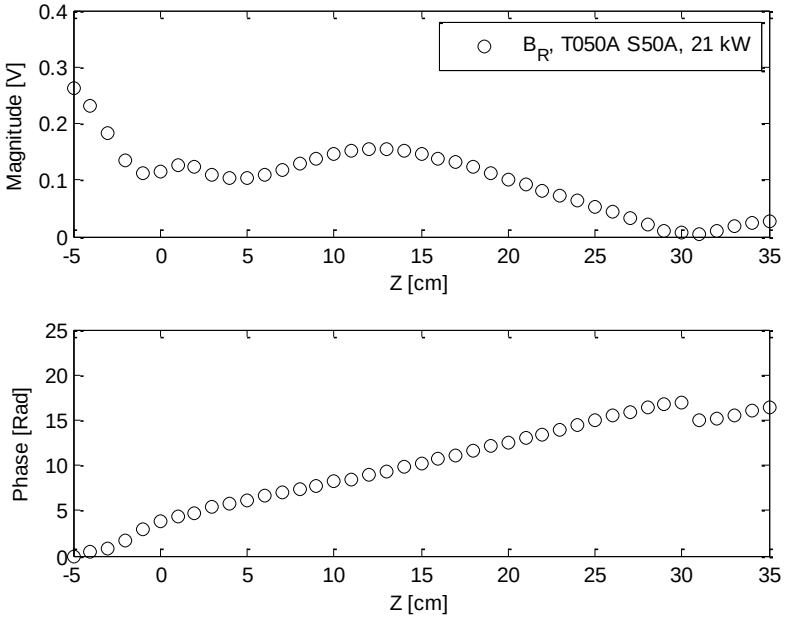

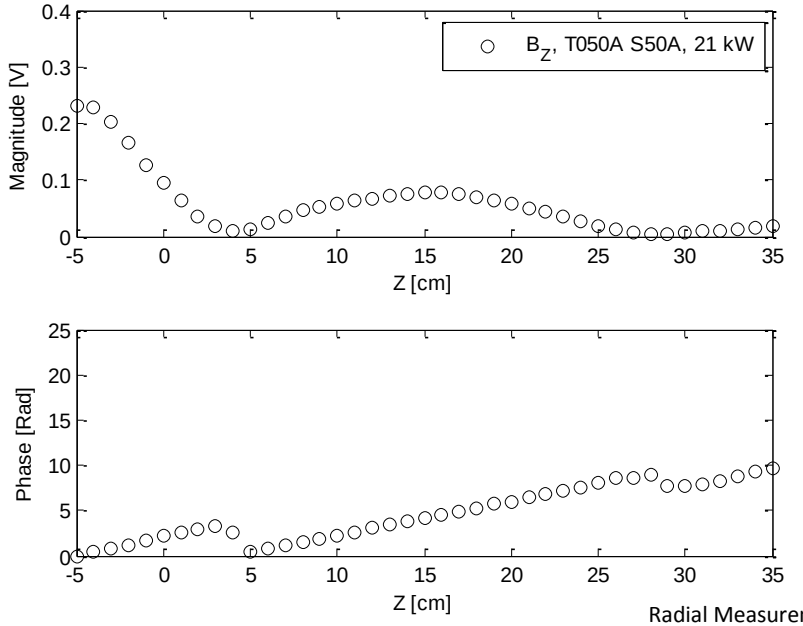

Radial Measurements >>

Radial field measurements

Increasing the magnetic mirror for constant RF power leads to:

- Increase in ion density
- Focusing of B_z component
- Excitation of high order radial modes

T450A S50A at 21 kW

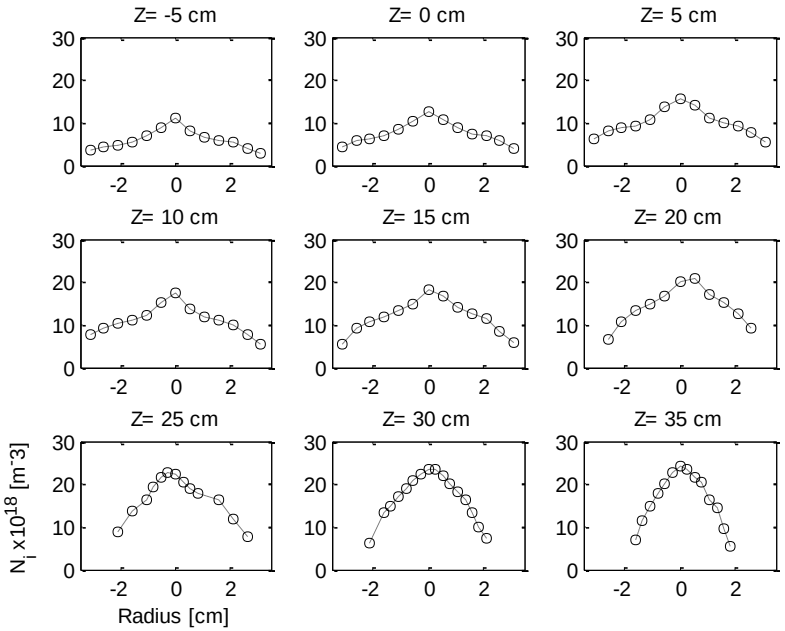

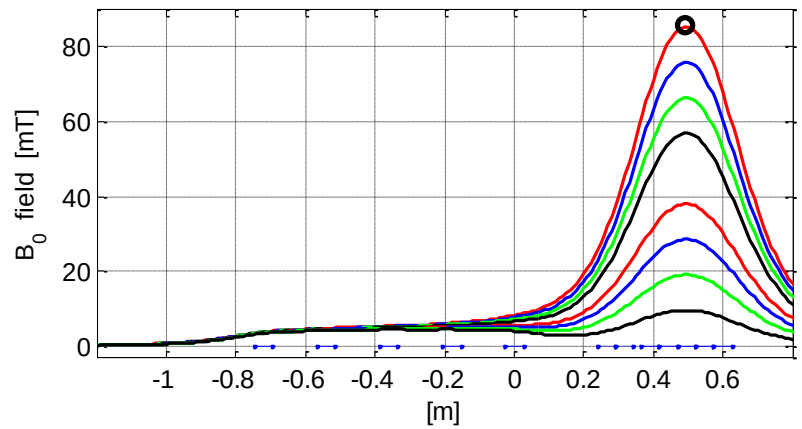

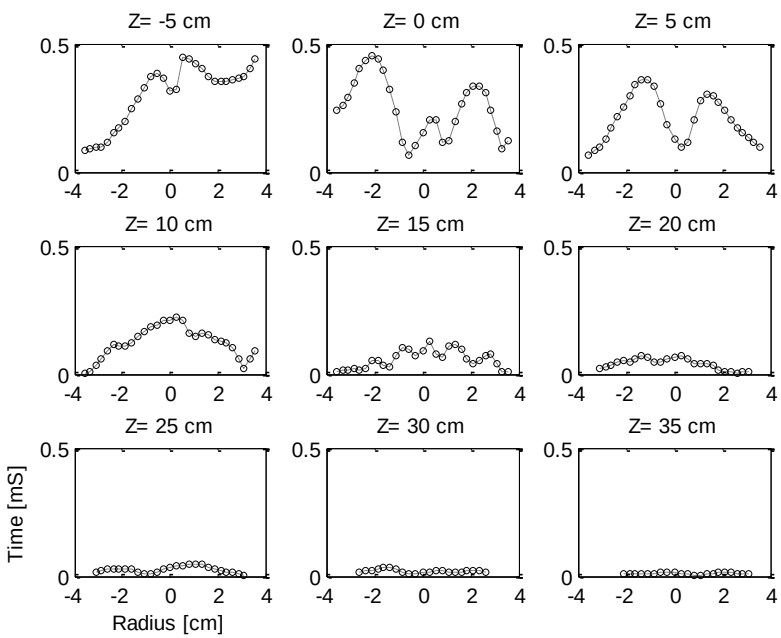

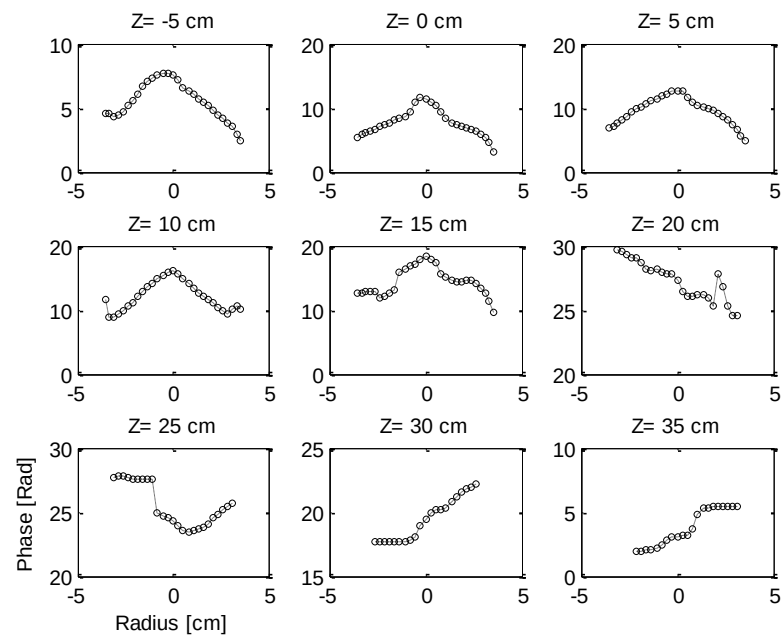

T400A S50A at 21 kW

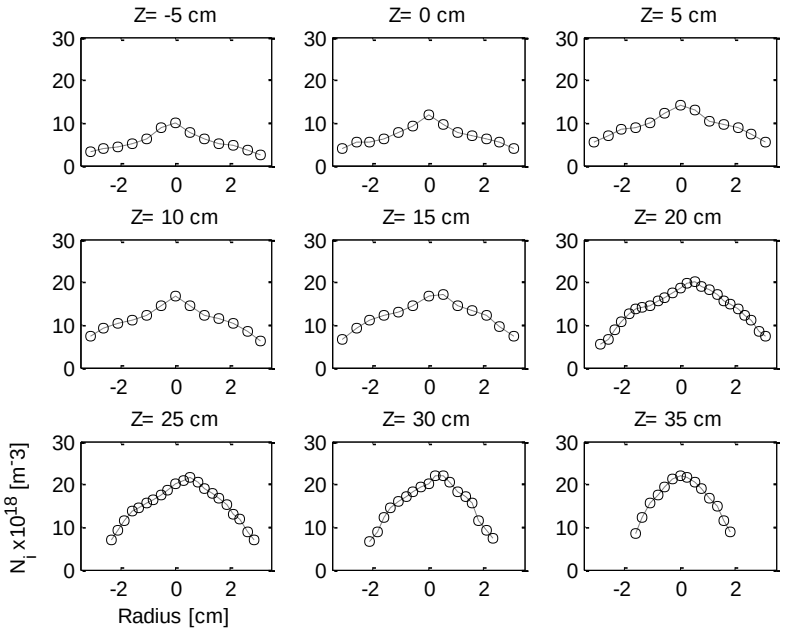

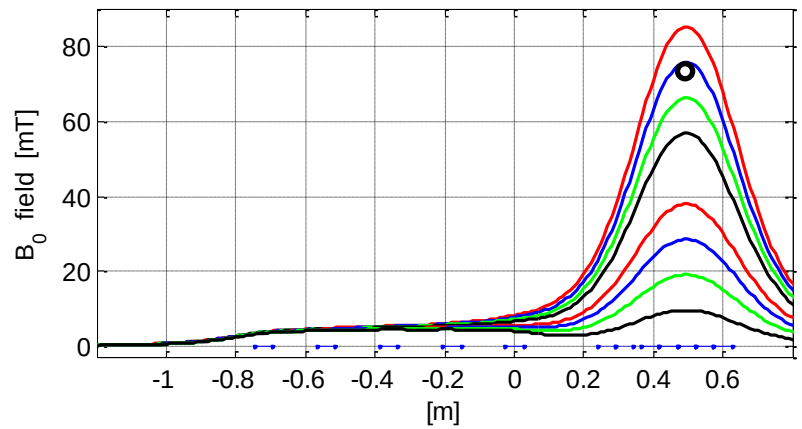

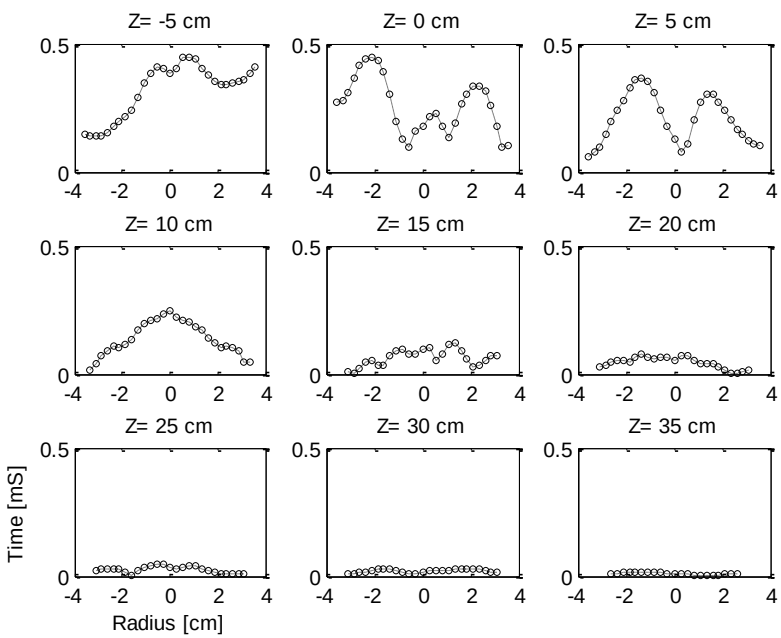

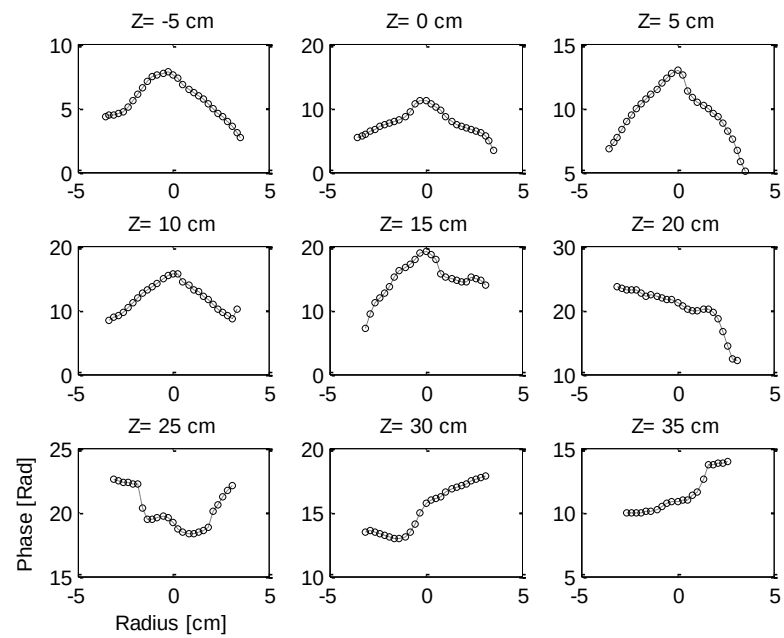

T350A S50A at 21 kW

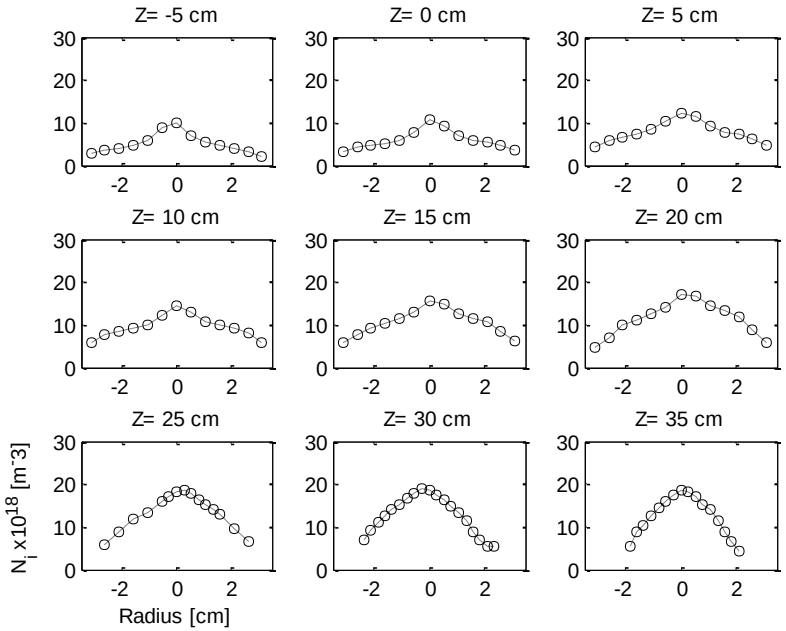

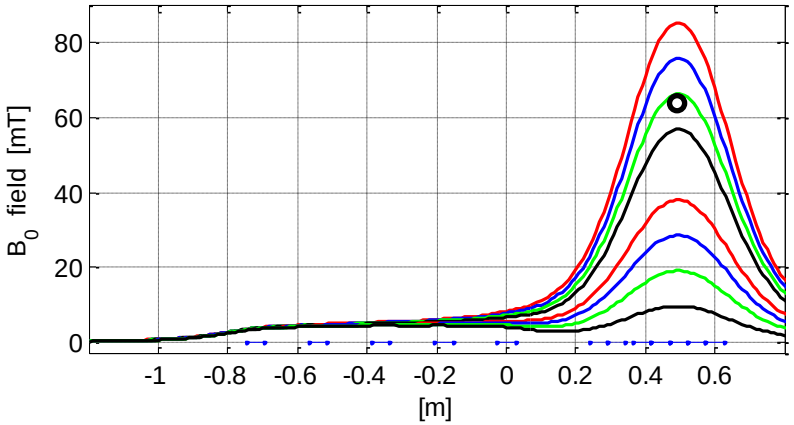

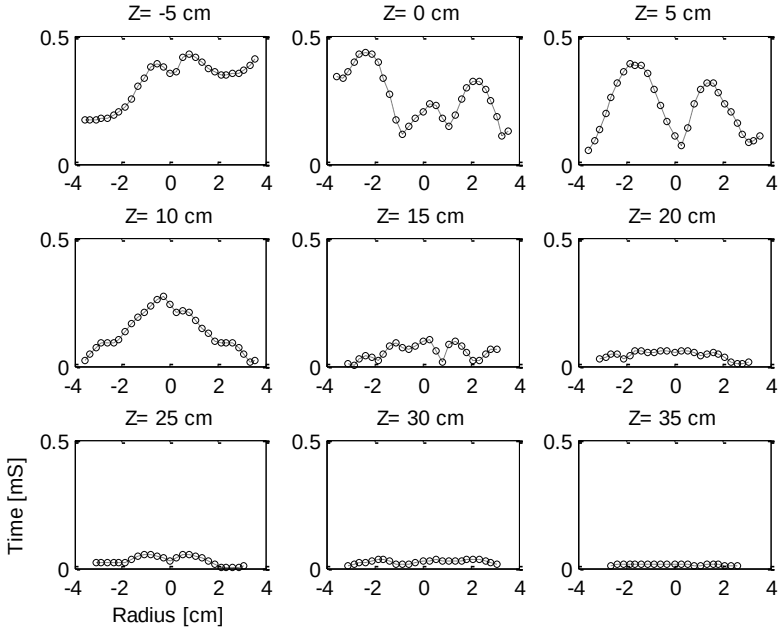

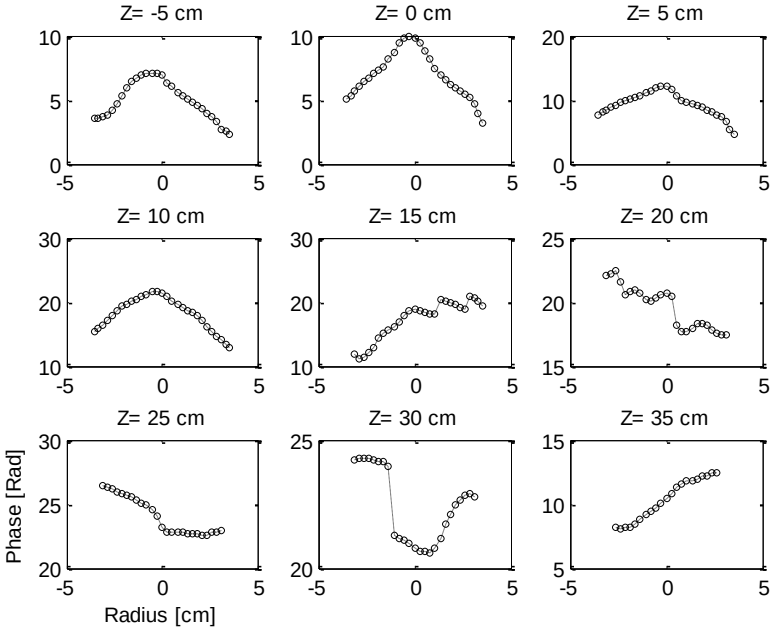

T300A S50A at 21 kW

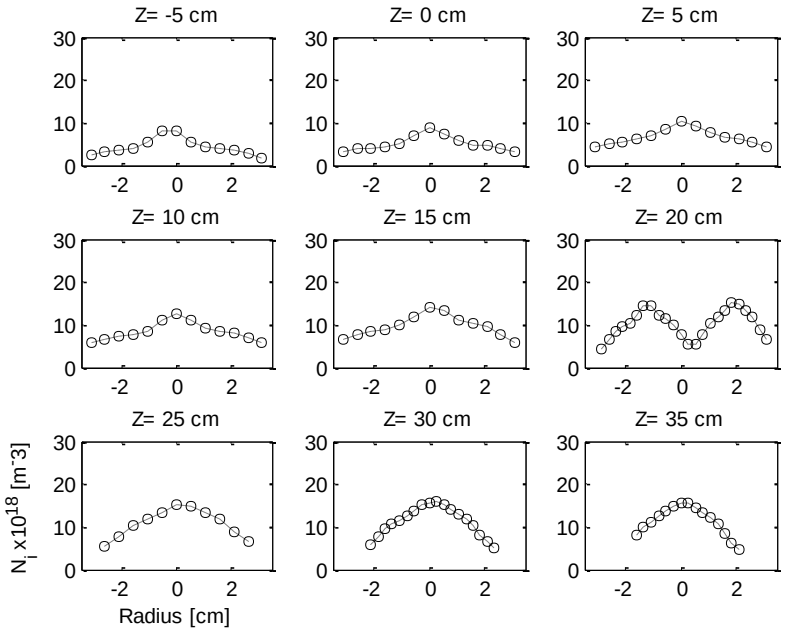

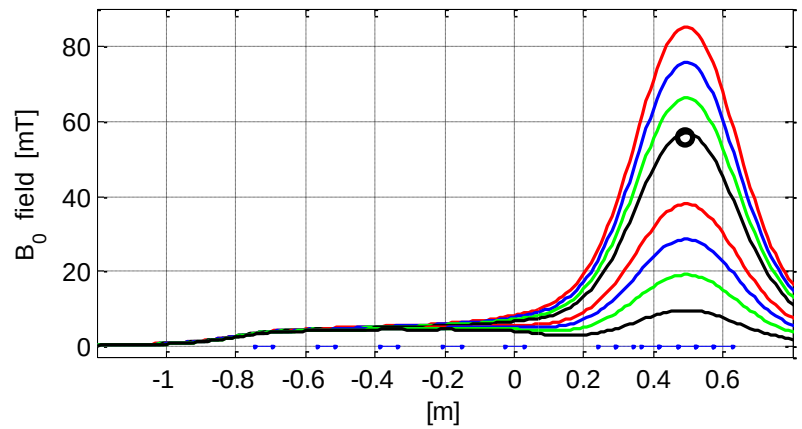

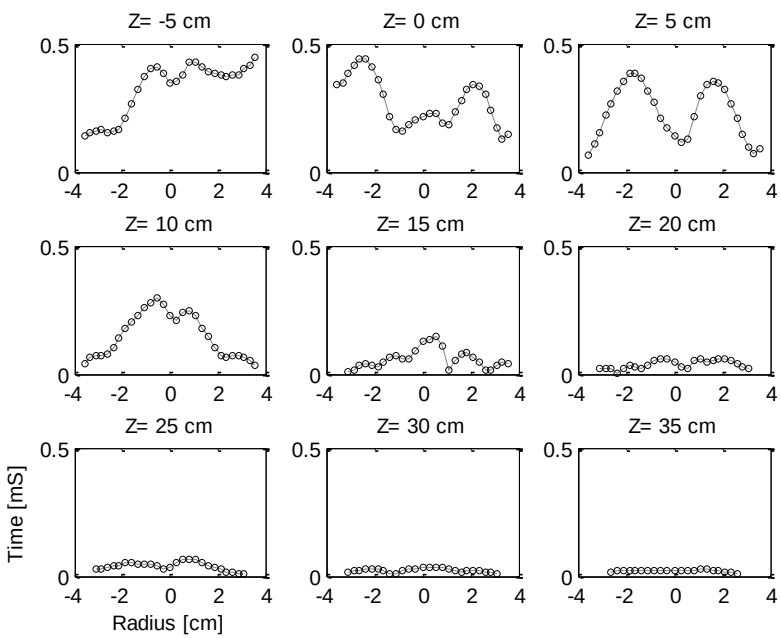

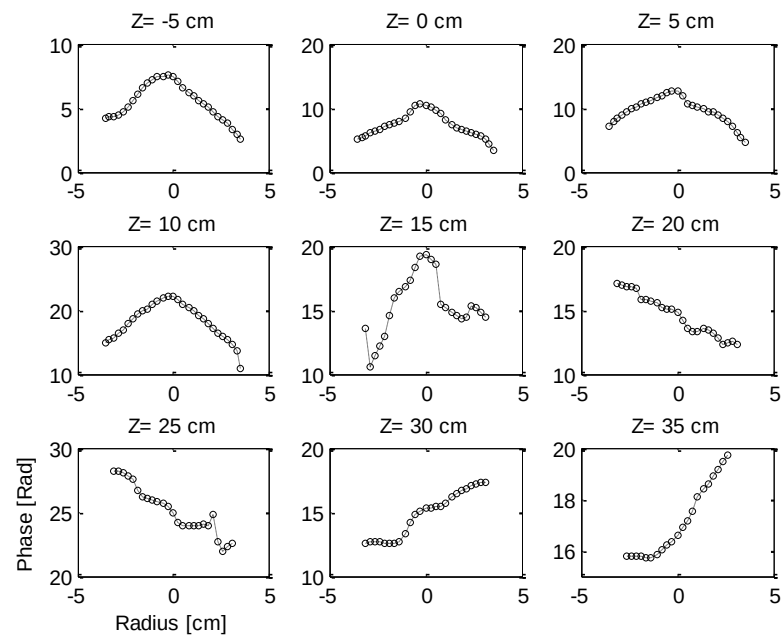

T200A S50A at 21 kW

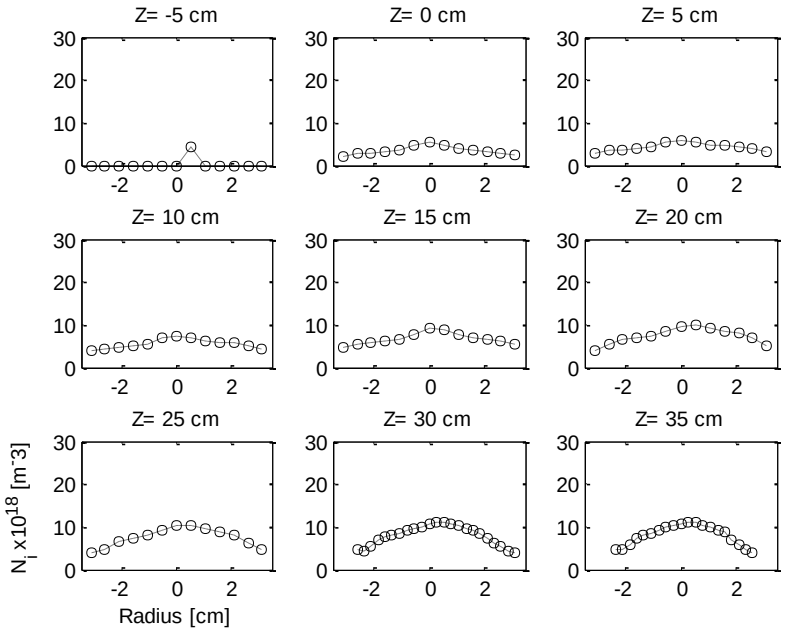

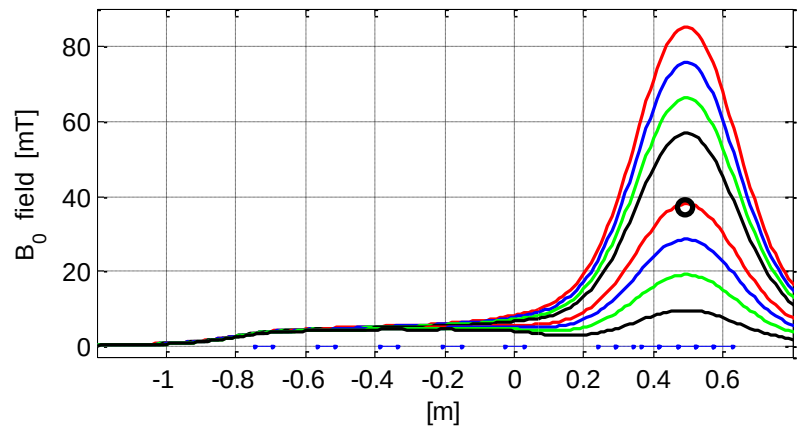

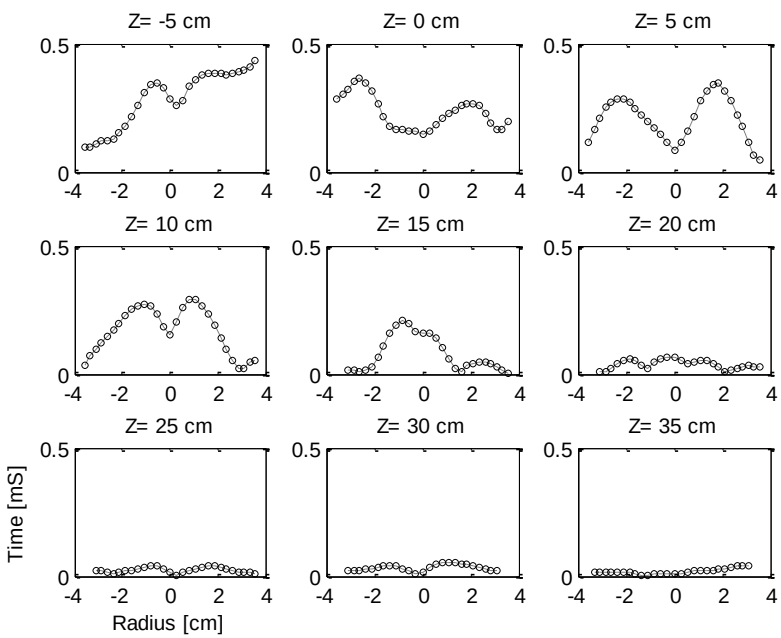

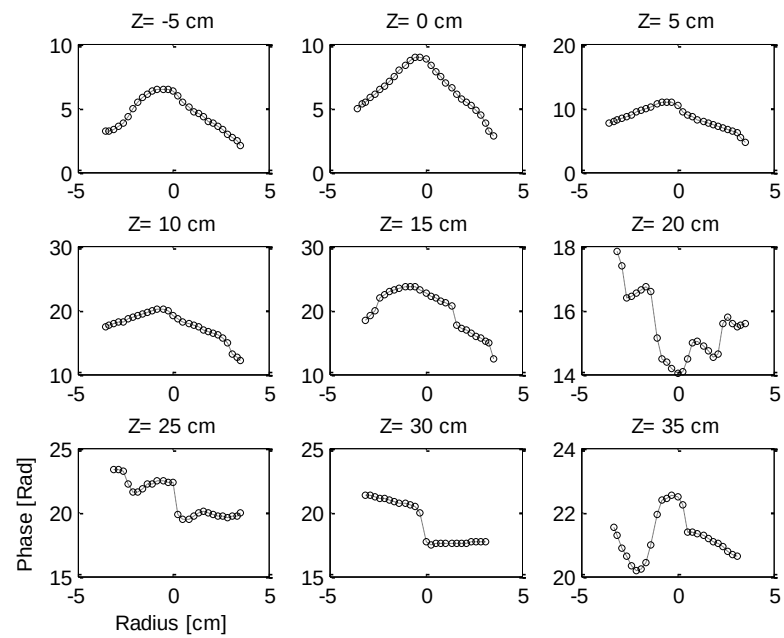

T150A S50A at 21 kW

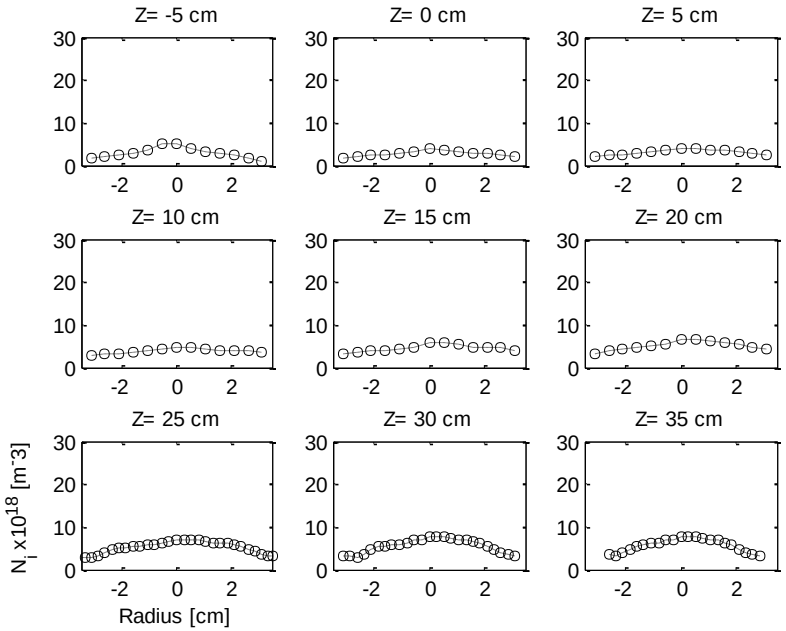

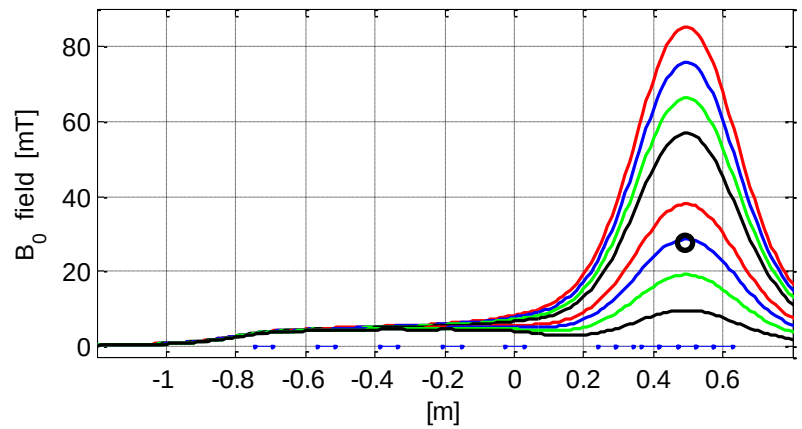

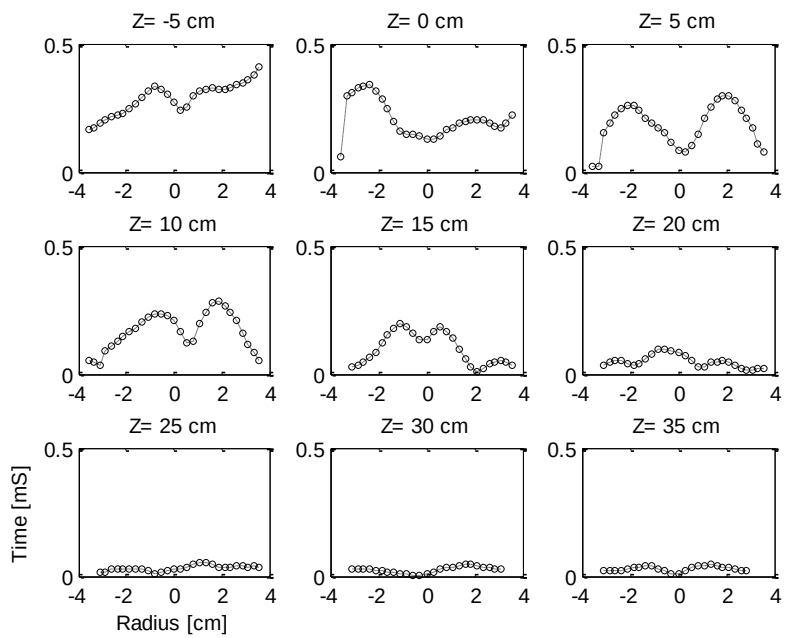

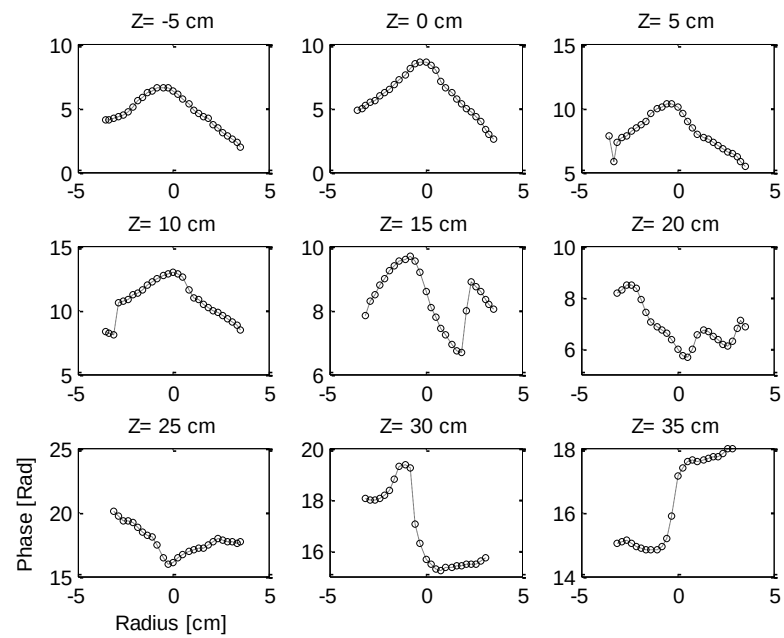

T100A S50A at 21 kW

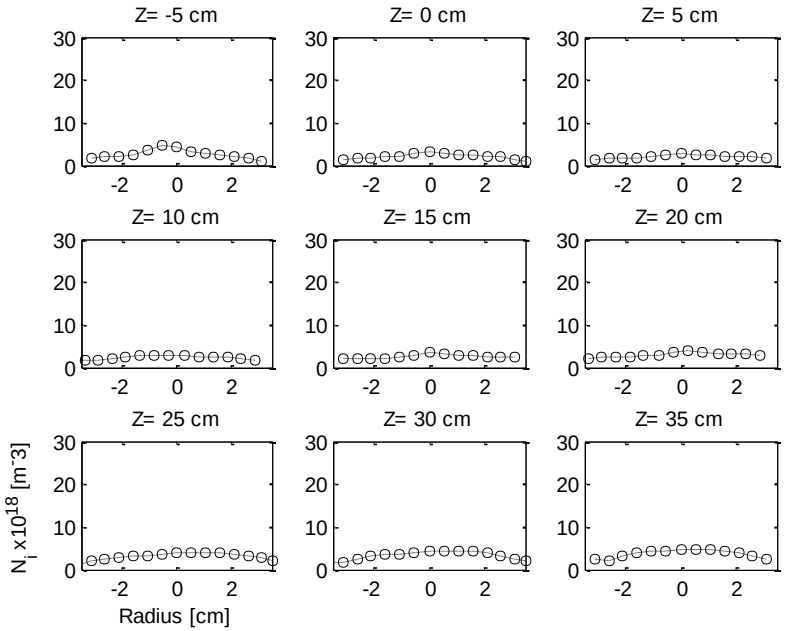

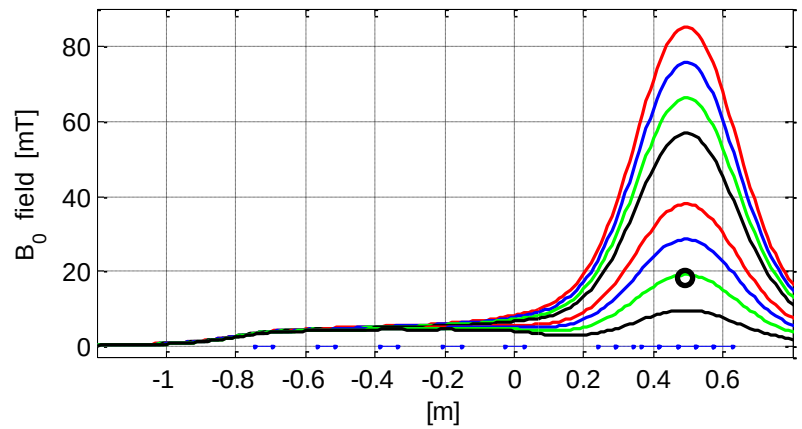

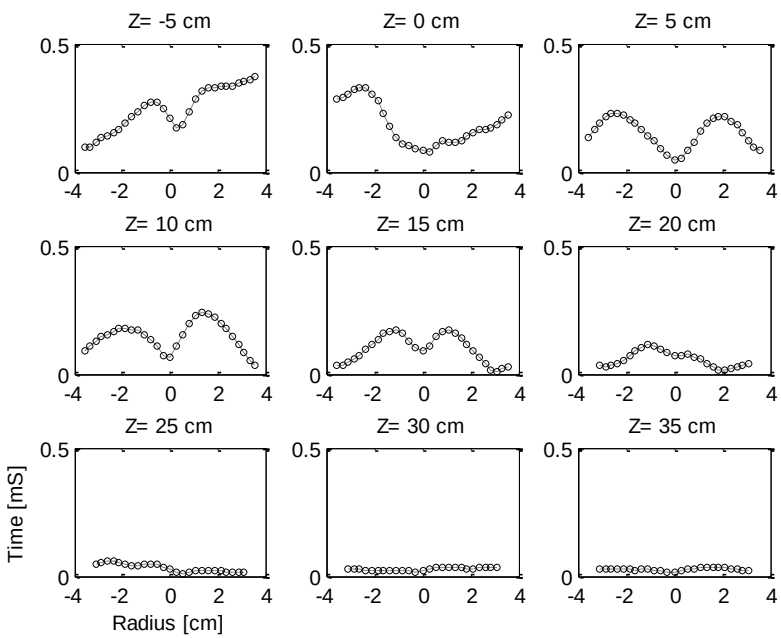

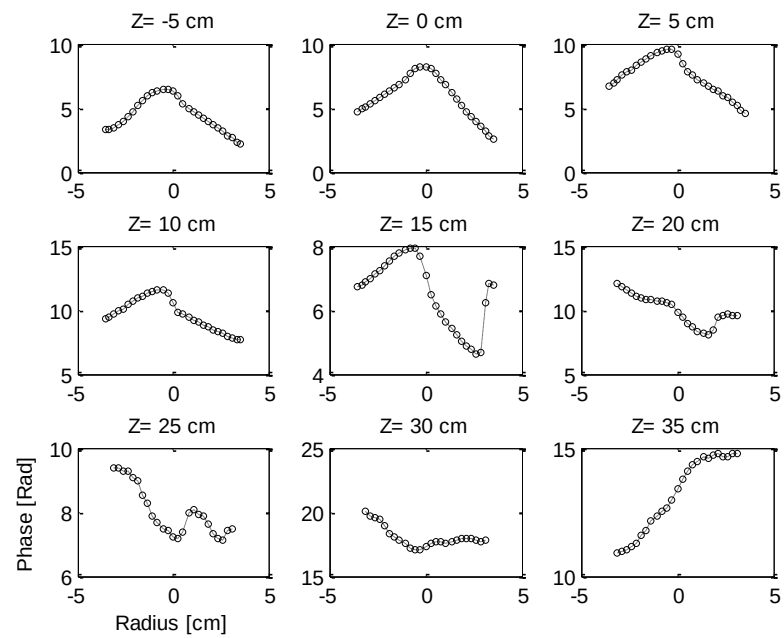

T050A S50A at 21 kW

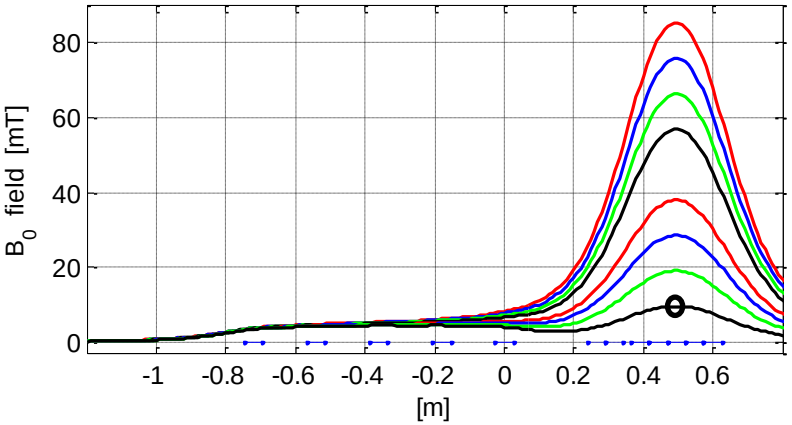

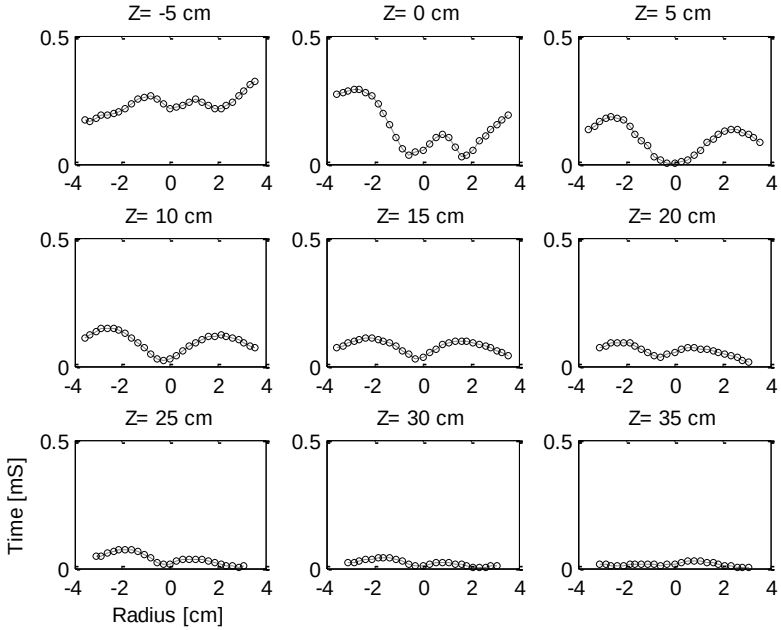

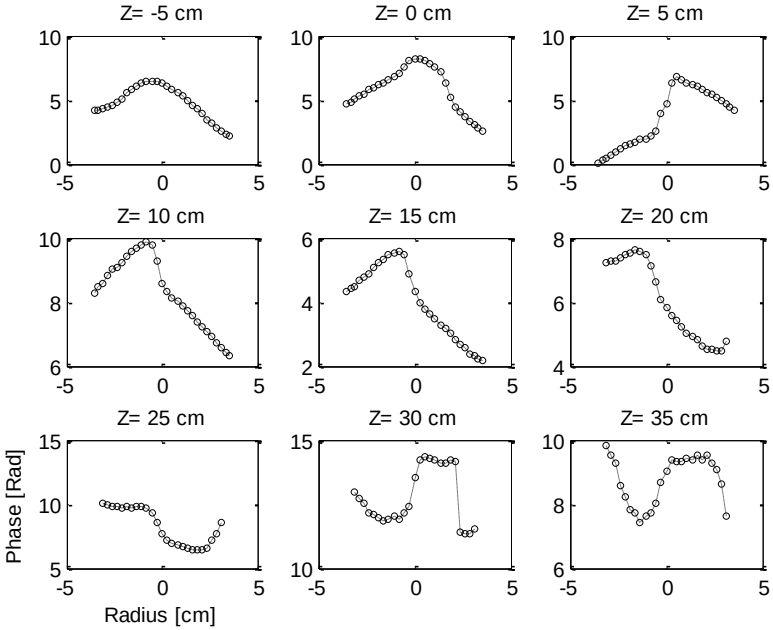

Summary >>

Summary:

- PMI in Fusion
- Intro to MAGPIE
- Diagnostics for Helicon wave studies
  - Interferometer
  - RF Bdot probe + IQ mixer system
  - RF double probe
    - RF compensation model
    - Insight into probe design.
- Propagation of helicon waves in magnetic mirrors at 20 kW in H_2
  - Focusing of helicon wave fields
  - Excitation of higher order radial modes
  - Smaller probe required to resolve higher order modes

Future work:

- Investigate the behavior of plasma density and electron temperature over a larger parameter space:
  - Magnetic field strength
  - Source field
  - Gas species and fill pressure.
  - RF power

- Dispersion relation of helicon waves with data available. Compare with Radial localized helicons and standard helicons

- Numerical electromagnetic simulations with the above data. Observe the presence of anomalous (non classical) wave damping over the parameter space.

References:

“Design and characterization of the Magnetized Plasma Interaction Experiment (MAGPIE): a new source for plasma–material interaction studies,”
B. D. Blackwell, **J. F. Caneses**, C. M. Samuell, J. Wach, J. Howard, and C. Corr, *Plasma Sources Sci. Technol.*, vol. 21, no. 5, p. 055033, Oct. 2012.

Additional material:

Time evolution of ion density radial profile:

- Standard magnetic field, z = 17 cm
- Early inductive discharge component at high RF power.
- Triangular shaped density profiles above 9 kW, characteristic of helicon heated plasma
- At low power density profile is broad
- In all cases, steady state is achieved at about 0.5 mS

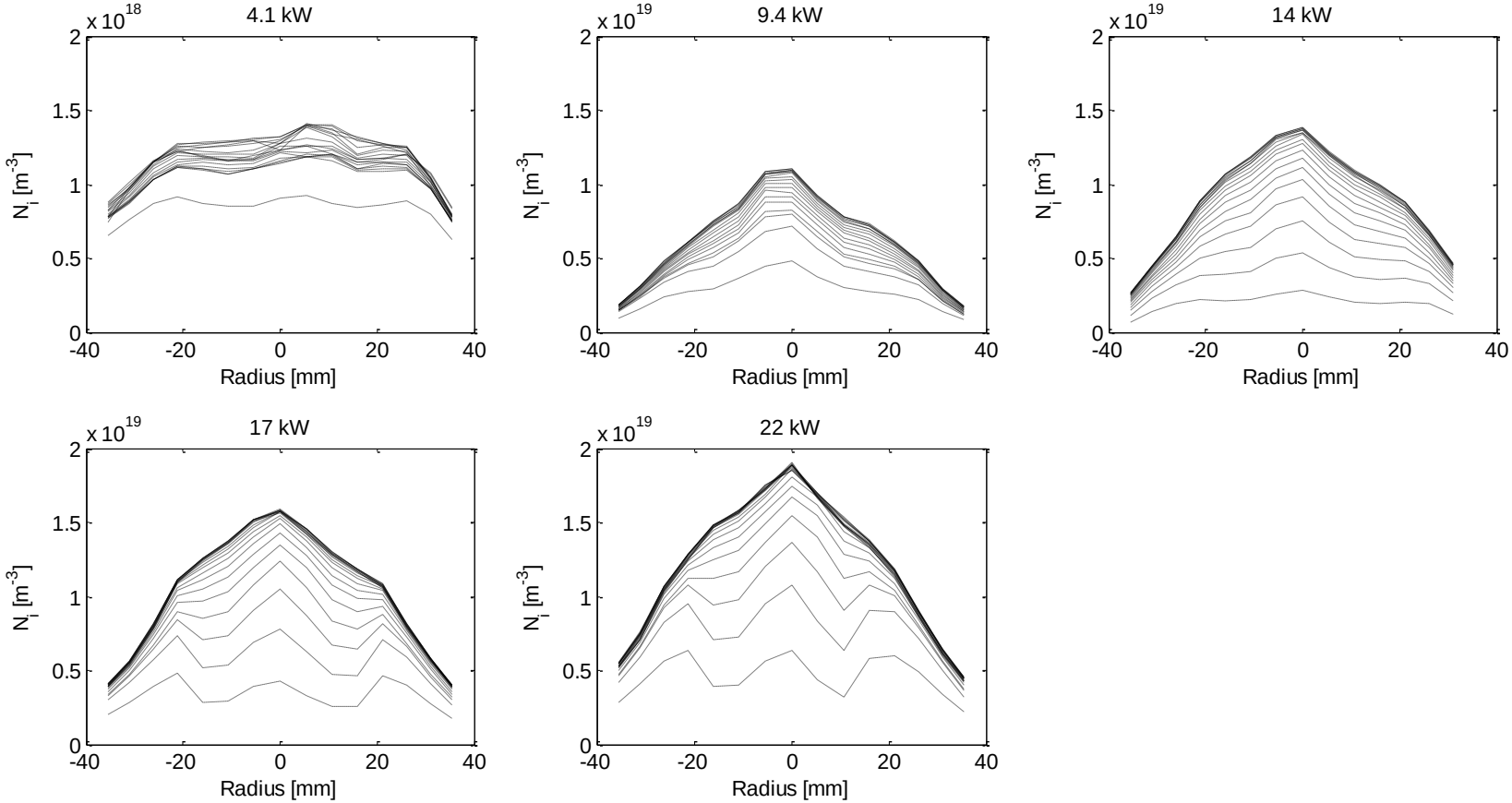

Time evolution of ion density radial profile:

- Standard magnetic field, z = 17 cm

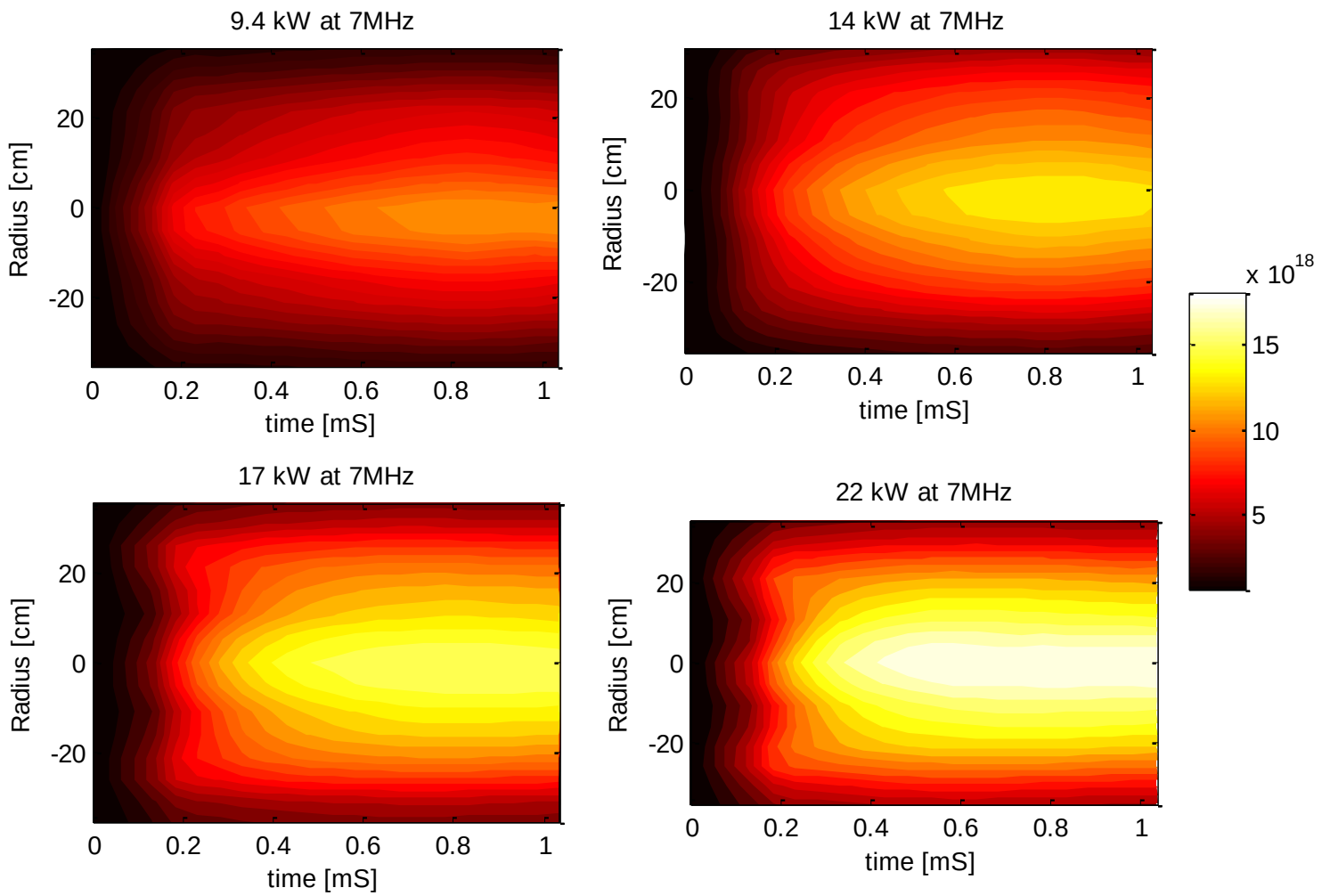

Changing magnetic field geometry

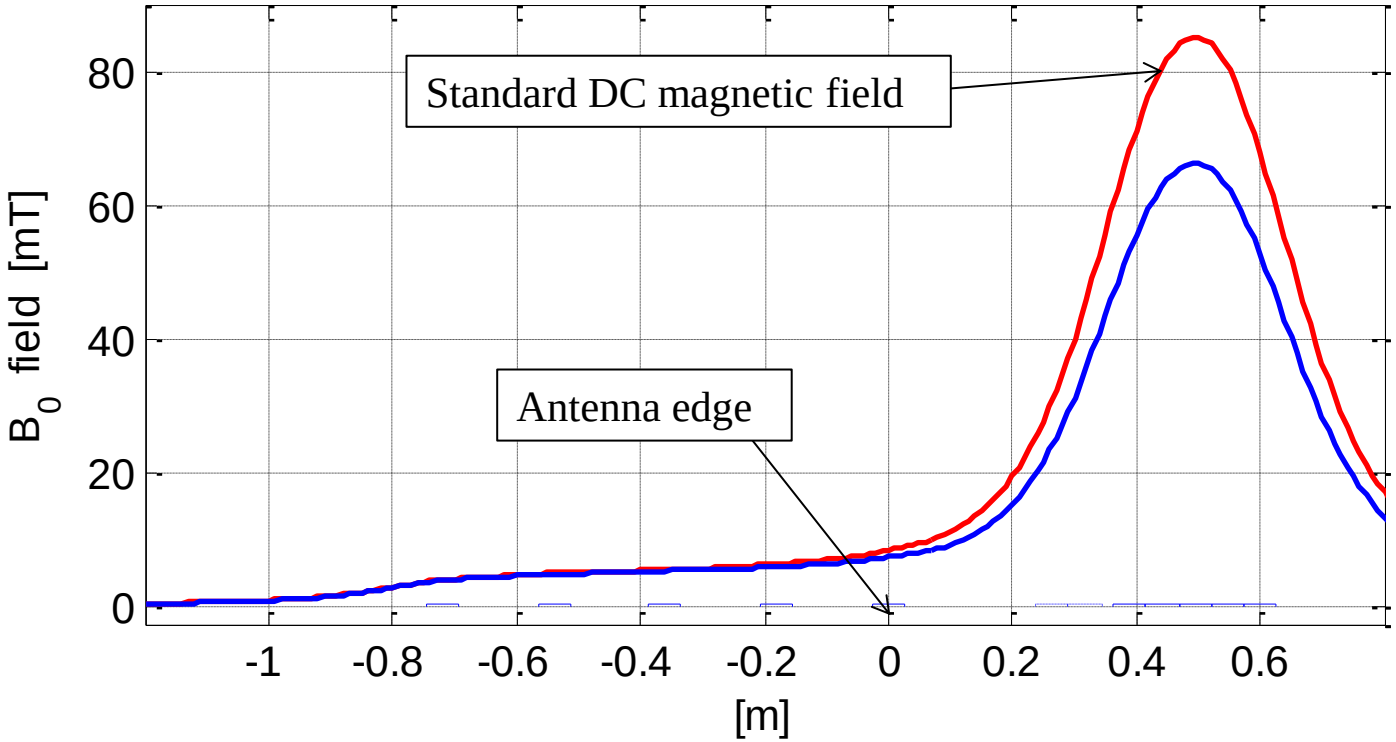

- Change mirror field currents: 450 and 350 A,
- Source current 50 A for all

Time evolution of ion density axial profile T450 S50:

- Mirror field currents: 450 A
- Source current 50 A
- 20 kW, H_2 8 mTorr

- Density peak at 30 cm late in time, maximum density ~1.8e19
- Temperature monotonically decreases in space, maximum temperature ~ 6 eV

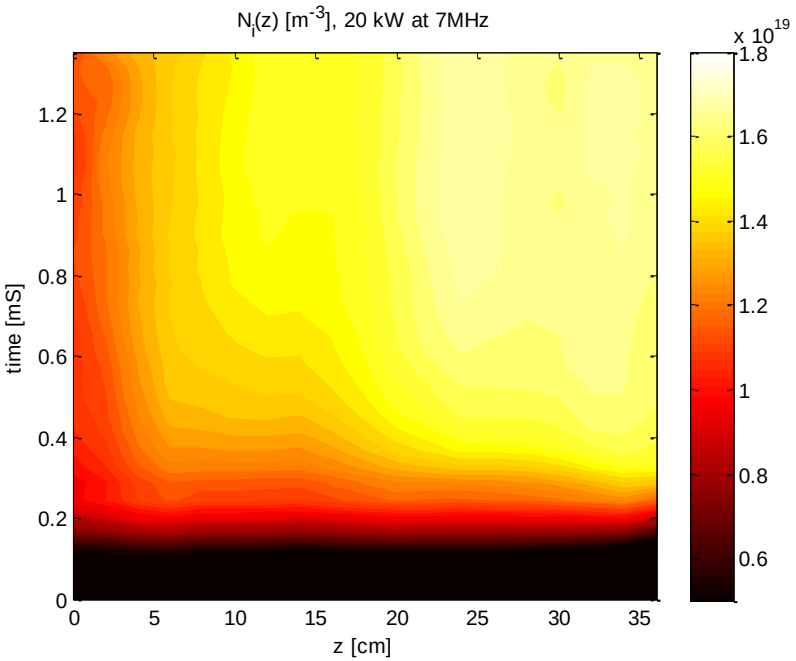

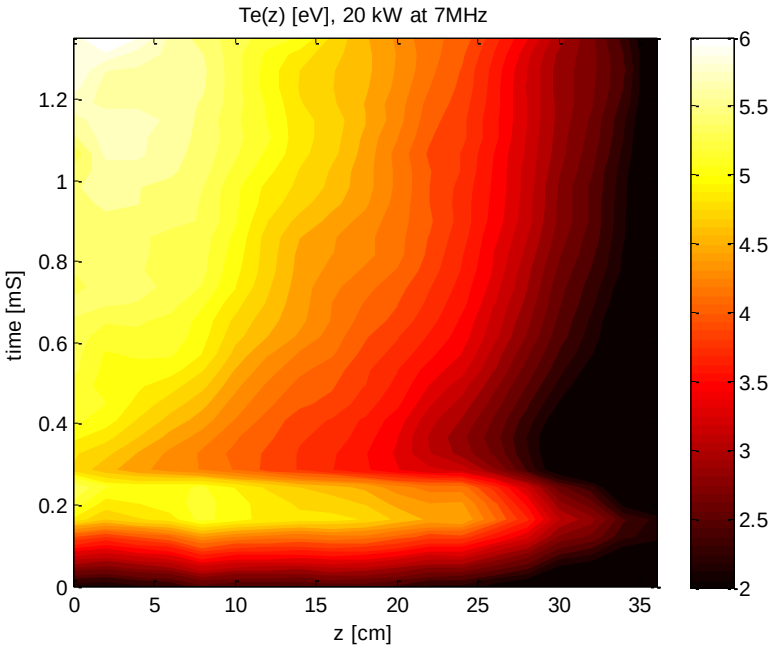

Time evolution of ion density axial profile T350 S50:

- Mirror field currents: 350 A
- Source current 50 A
- 20 kW, H_2 8 mTorr

- Density peak at 30 cm late in time, maximum density ~1.4e19
- Temperature monotonically decreases in space, maximum temperature ~ 6 eV

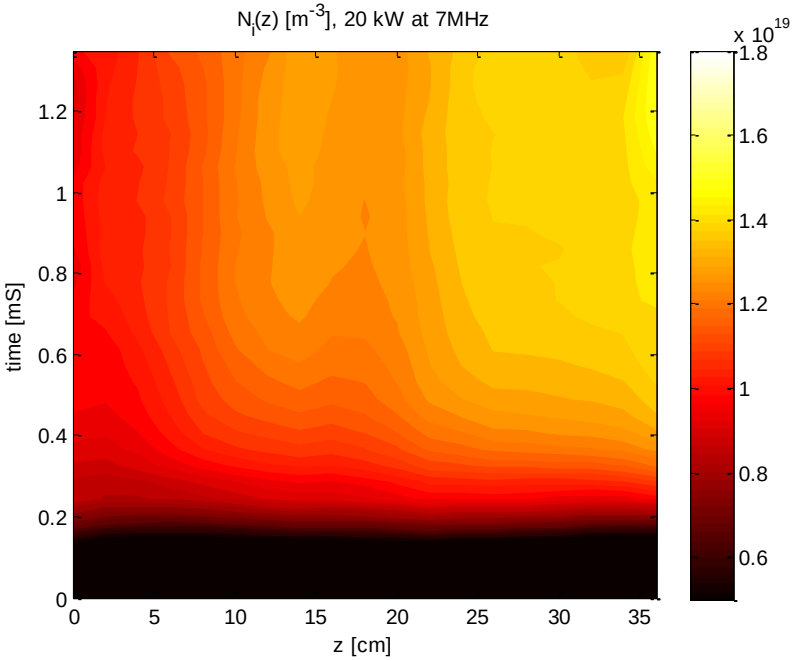

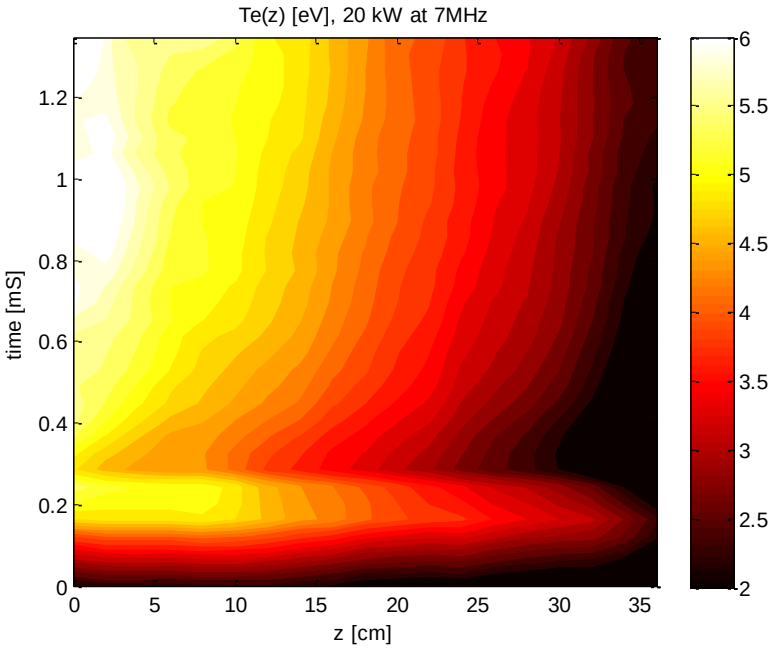

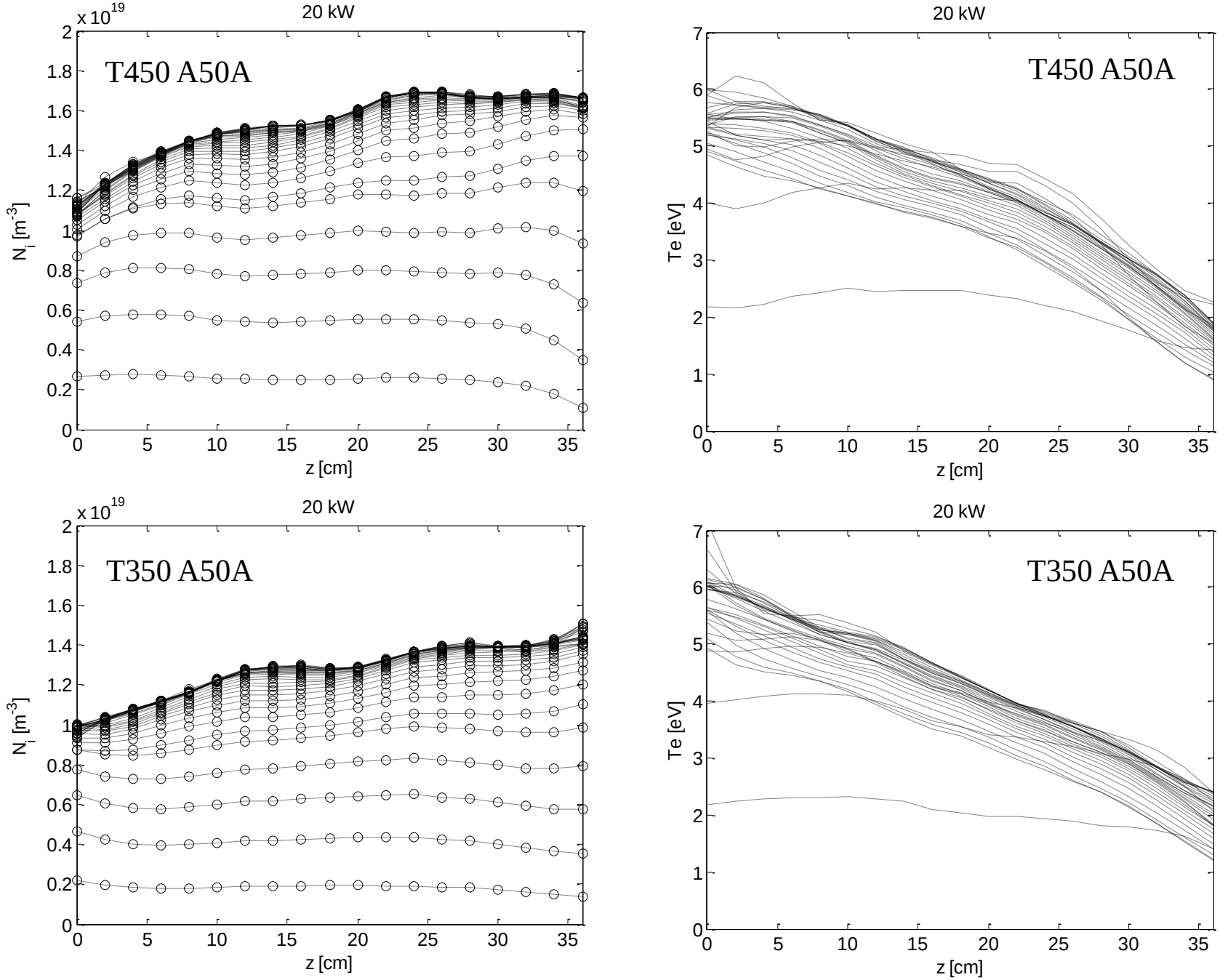
20 kW
x 10^19
T450 A50A
N_i [m^-3]
z [cm]
20 kW
T450 A50A
Te [eV]
z [cm]
20 kW
x 10^19
T350 A50A
N_i [m^-3]
z [cm]
20 kW
T350 A50A
Te [eV]
z [cm]

Plasma Material interaction studies in MAGPIE:

Graphite:

Physical to chemical erosion of graphite in hydrogen/Argon plasma

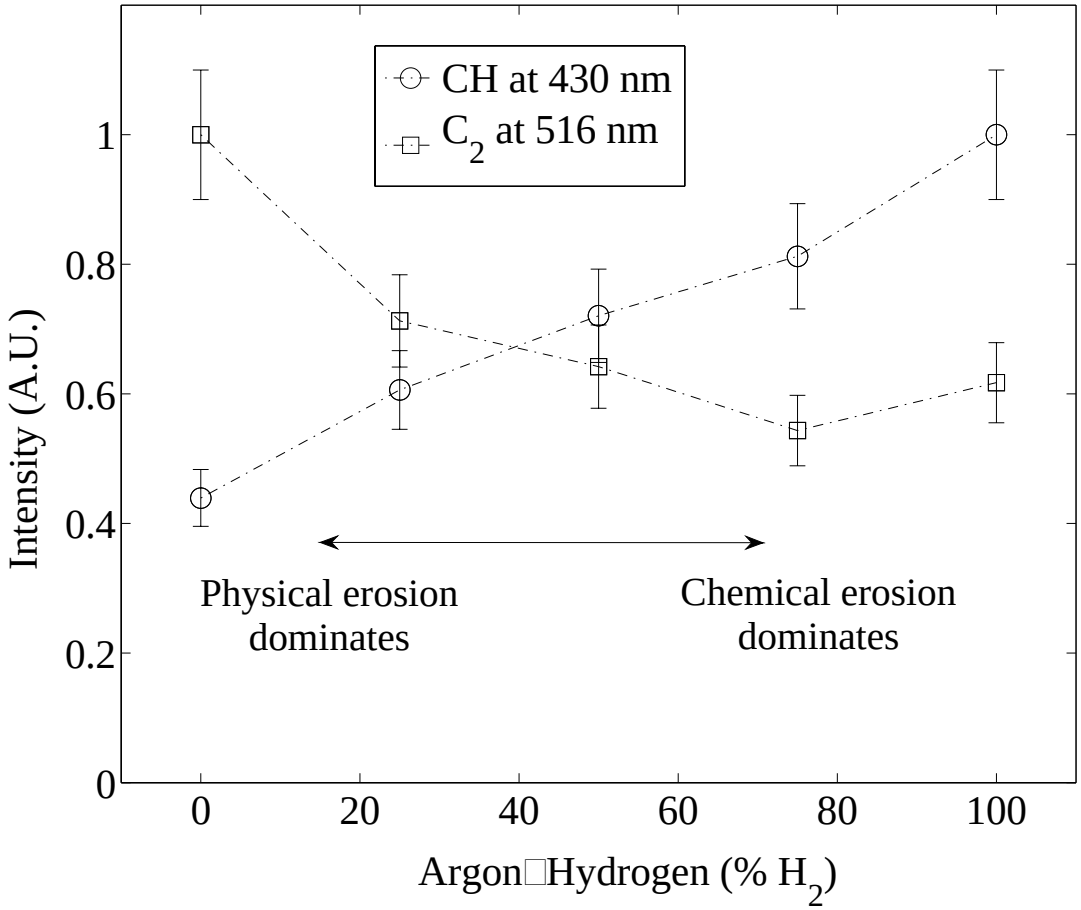

Plasma Material interaction studies in MAGPIE:

Tungsten:

- Blistering on the surface.

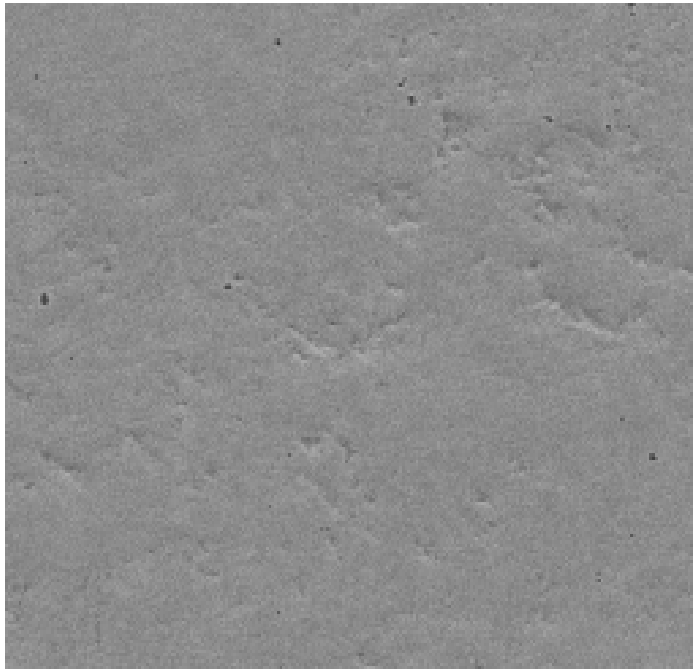

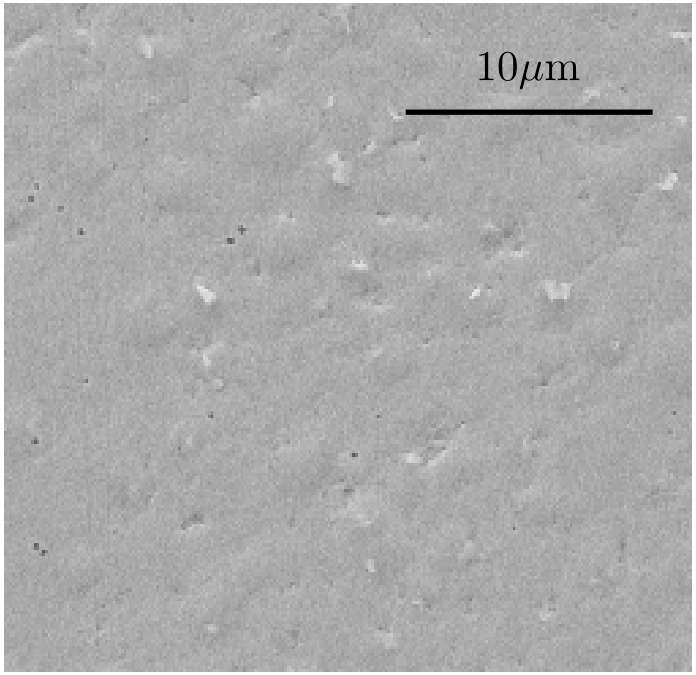

Gas: Helium

$p = 4\text{mTorr}$

$P = 500\text{W}$

$|B| \sim 50\text{G}$

$V_{\text{bias}} = -250V$

Ion dose $\sim 10^{19}$ ions cm^{-2}

Plasma Material interaction studies in MAGPIE:

Tungsten:

- Increases plasma density in He and heated target
- Blister formation in He plasma exposed tungsten, thickness ~ 175 nm
- Plasma density ~ 5 x 10^{17} m^{-3}
- Target temperature ~ 150 ^{o}C

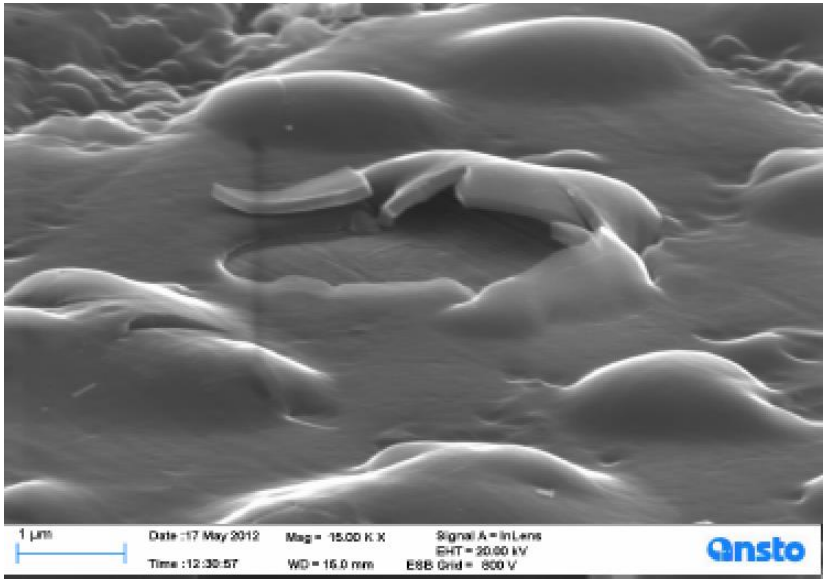

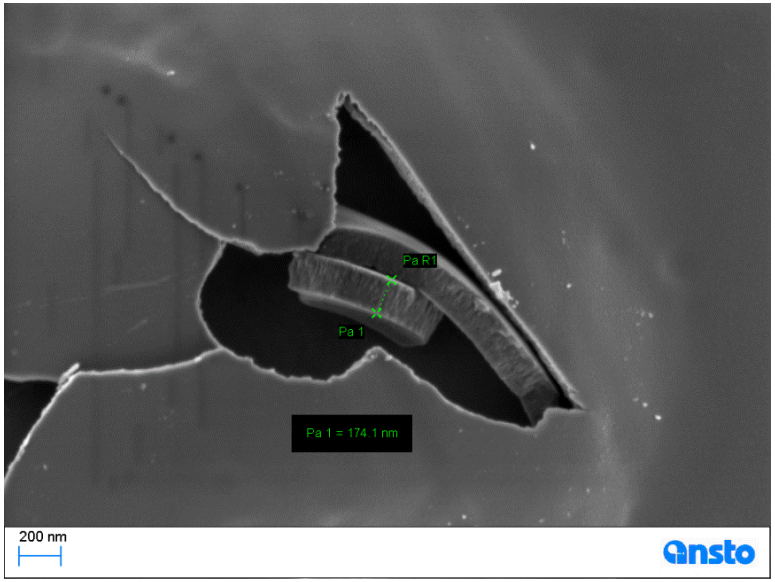

Plasma Material interaction studies in MAGPIE:

Diamond :
(a) and (b) before exposure to plasma,
(c) and (d) after plasma exposure, sample bias -375 V.

Inset of (b) and (d) shows terrace-like features that are resolved after plasma exposure.

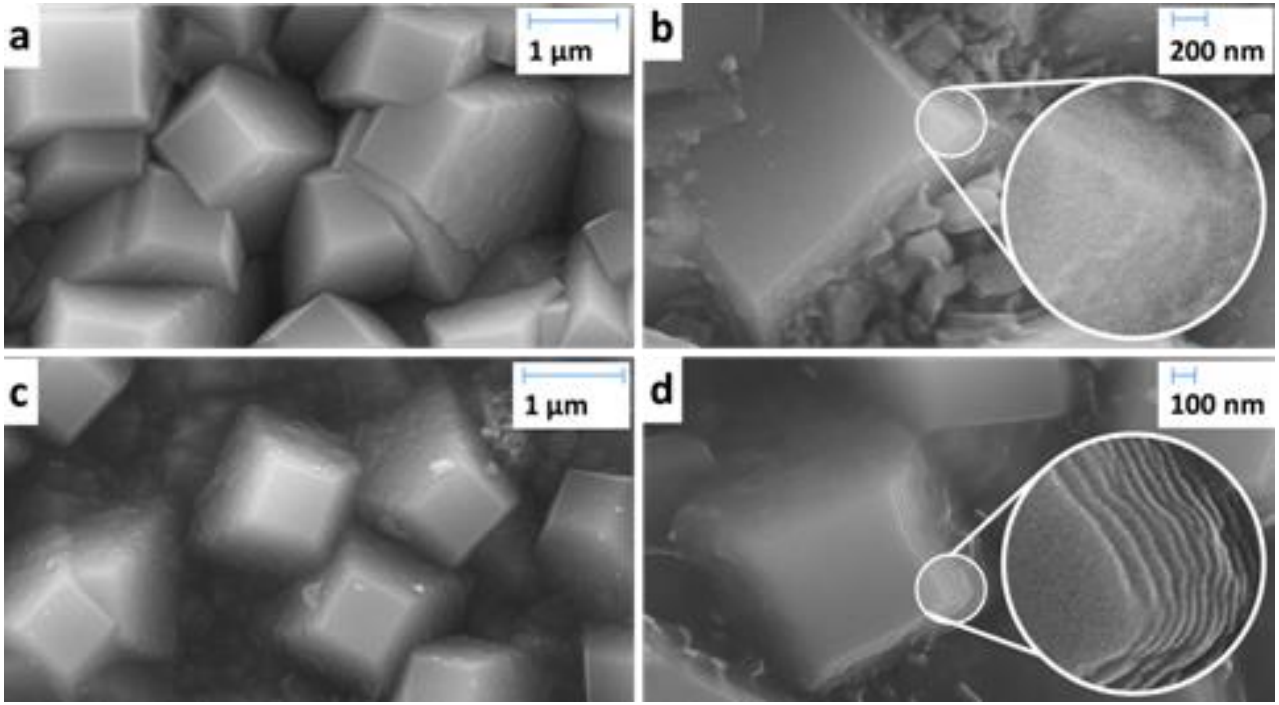

REF: Deslandes et al. Submitted to Journ. Nucl. Materials (2013)

T400A S50A
21 kW

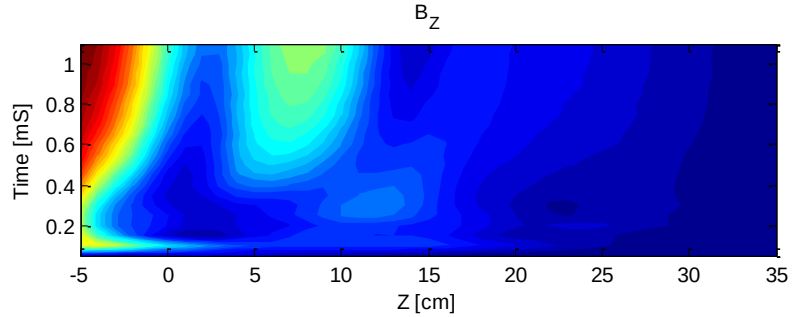

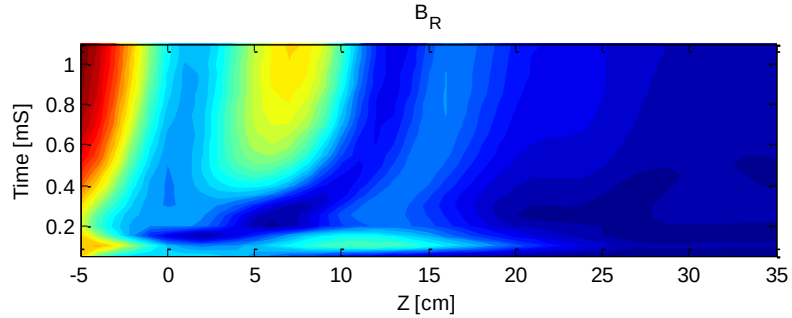

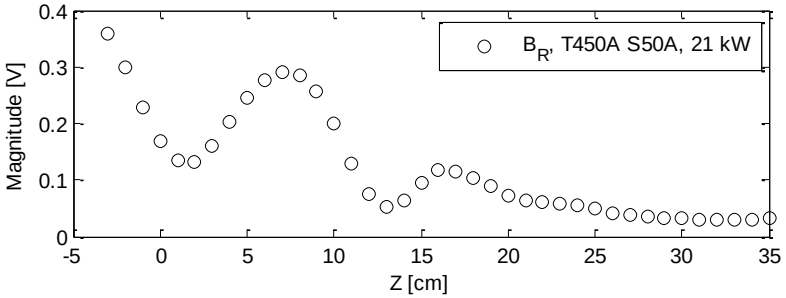

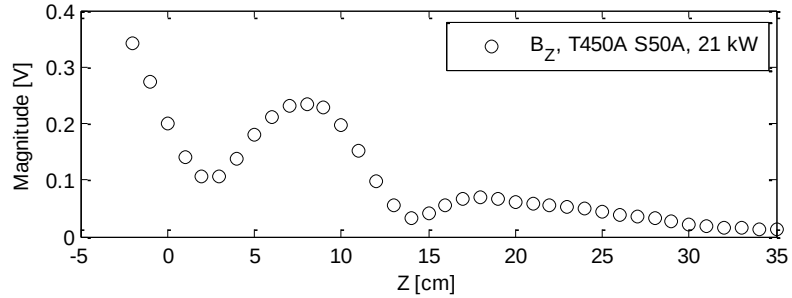

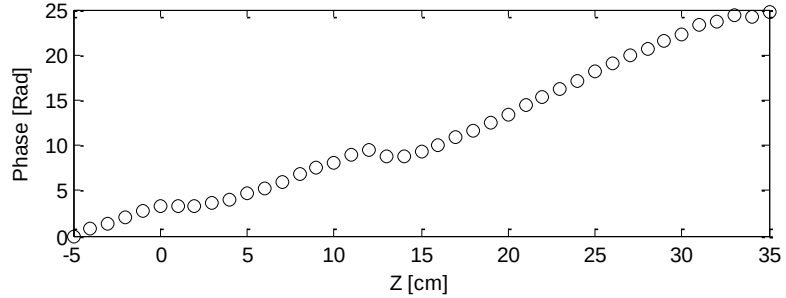

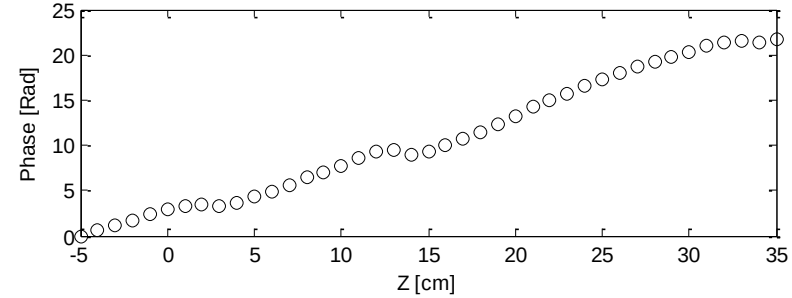
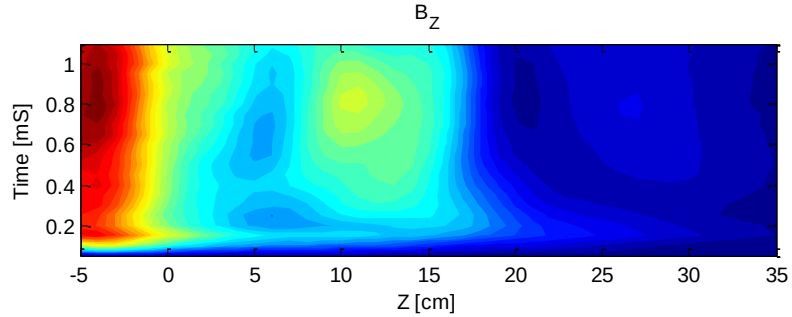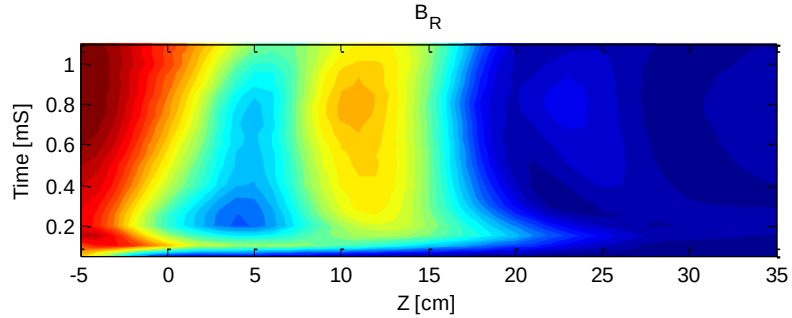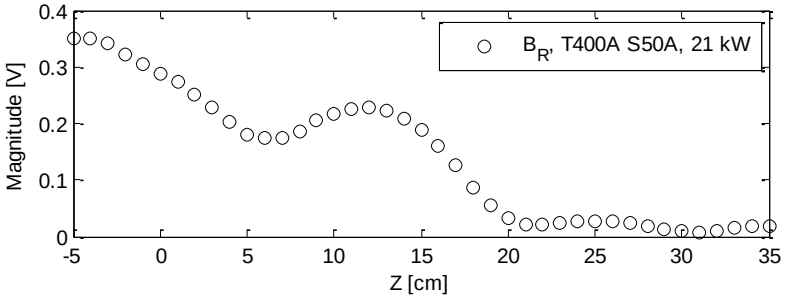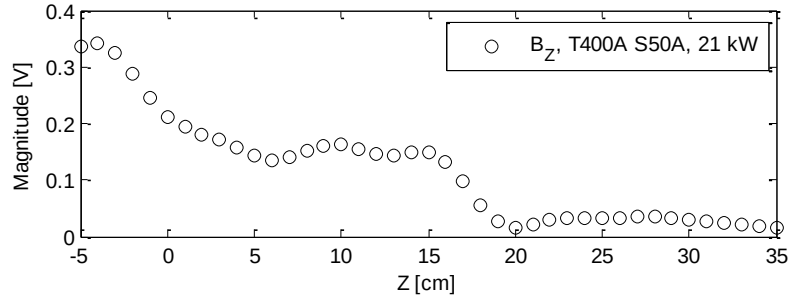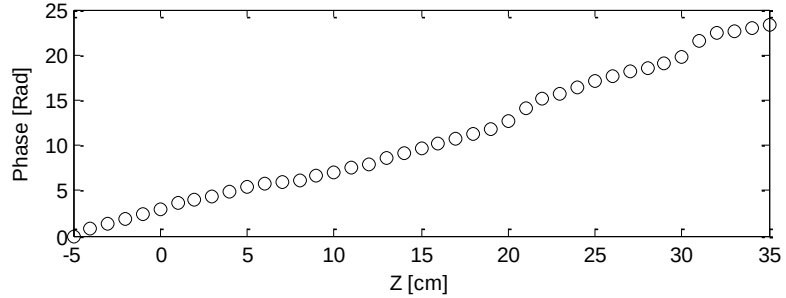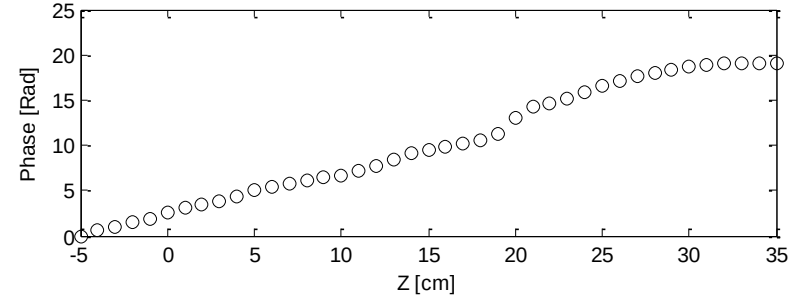
T400A S50A
12 kW